SANDIA REPORT
SAND2017-9099
Unlimited Release
Printed August 2017

Subsequent R + O_2 Chemistry of Intermediates Formed in Low-Temperature R + O_2 Reactions: Potential Importance in Modeling Autoignition Behavior

Brandon Rotavera, Rebecca L. Caravan and Craig A. Taatjes

Prepared by
Sandia National Laboratories
Albuquerque, New Mexico 87185 and Livermore, California 94550

Sandia National Laboratories is a multimission laboratory managed and operated by National Technology and Engineering Solutions of Sandia, LLC, a wholly owned subsidiary of Honeywell International, Inc., for the U.S. Department of Energy's National Nuclear Security Administration under contract DE-NA0003525.

Issued by Sandia National Laboratories, operated for the United States Department of Energy by National Technology and Engineering Solutions of Sandia, LLC.

Available to DOE and DOE contractors from
U.S. Department of Energy
Office of Scientific and Technical Information
P.O. Box 62
Oak Ridge, TN 37831

Telephone: (865) 576-8401
Facsimile: (865) 576-5728
E-Mail: reports@osti.gov
Online ordering: http://www.osti.gov/scitech

Available to the public from
U.S. Department of Commerce
National Technical Information Service
5301 Shawnee Rd
Alexandria, VA 22312

Telephone: (800) 553-6847
Facsimile: (703) 605-6900
E-Mail: orders@ntis.gov
Online order: http://www.ntis.gov/search

SAND2017-9099
Printed August 2017
Unlimited Release

Subsequent R + O_2 Chemistry of Intermediates Formed in Low-Temperature R + O_2 Reactions: Potential Importance in Modeling Autoignition Behavior

Brandon Rotavera, Rebecca L. Caravan and Craig A. Taatjes
Combustion Chemistry Department
Sandia National Laboratories
P.O. Box 9055
Livermore, California 94551-0969

Abstract

Comprehensive chemical kinetics models used in the simulation of hydrocarbon and biofuel oxidation rely on accurate prescription of the underlying reaction mechanisms and rate parameters of associated elementary reactions. For practical transportation fuels, such models contain thousands of elementary reactions, which collectively define chain-initiation, -propagation, -branching, and -inhibition pathways. In the low-temperature regime, below approximately 1000 K where R + O_2 reactions dominate, primary oxidation intermediates including cyclic ethers, carbonyls, and conjugate alkenes are formed in abundance via unimolecular decomposition of either chemically activated or thermalized radicals, specifically organic peroxy (ROO) or hydroperoxyalkyl species (QOOH). Experimental results from multiplexed photoionization mass spectrometry (MPIMS) experiments are detailed herein for several intermediates, derived initially from R + O_2 reactions of hydrocarbons and biofuels, and show that intermediate species formed in the initial steps of oxidation undergo similar reactions to those of the parent molecule, including through QOOH-mediated pathways. Products from QOOH decomposition via chain-inhibition and chain-propagation pathways, namely conjugate alkenes, carbonyls, and cyclic ethers, are detected directly. Despite such rich chemistry involving QOOH radicals, most comprehensive chemical kinetics models neglect the complete description of primary oxidation intermediates, and rather consider a restricted number of reaction pathways. It is suggested that exclusion of the details of the oxidation of these intermediate products may affect the interpretation of combustion simulations using such models.

ACKNOWLEDGMENTS

BR gratefully acknowledges current and former colleagues in the Combustion Chemistry Department at the Combustion Research Facility of Sandia National Laboratories: Craig A. Taatjes, David L. Osborn, Judit Zádor, Lenny Sheps, Howard A. Johnsen, Kendrew Au, Ivan O. Antonov, Ewa Papajak, Krupa Ramasesha, John D. Savee, Oliver Welz, Haifeng Huang, Adam M. Scheer, Ming-Wei Chen and Arkke J. Eskola. The work herein was supported by the Department of Energy under Award Number DE-PI0000012, the U.S-China Clean Energy Research Center (CERC) Clean Vehicle Consortium.

CONTENTS

FIGURES

TABLES

NOMENCLATURE

DOE	Department of Energy
HO_2	hydroperoxyl radical
MPIMS	multiplexed photoionization mass spectrometry
nm	nanometer
NTC	negative temperature coefficient (region)
OH	hydroxyl radical
QOOH	hydroperoxyalkyl radical
ROO/RO_2	organic peroxy radical
SNL	Sandia National Laboratories

1. INTRODUCTION

The comprehensive chemical kinetics models that are used to simulate combustion chemistry span thousands of species and elementary reactions in order to predict the complex pressure- and temperature-dependence of reaction pathways that govern pollutant formation and autoignition [1-6]. Central to the predictive capabilities of such models are accurate rate parameters for the constituent elementary reactions and inclusion of all significant radicals and intermediates formed during incipient and subsequent oxidation steps. In the low- and intermediate-temperature regimes of combustion (below ~1000 K), where the carbon skeleton of the parent molecule can remain intact during the initial oxidation steps, the driving sequence of chain-branching reactions leading to autoignition is derived from (first) O_2-addition to organic radicals (R), which are formed from the fuel via H-abstraction, principally by OH. Subsequent isomerization of the ensuing oxygen-centered alkylperoxy radicals (ROO) leads to carbon-centered hydroperoxy-substituted organic radicals (QOOH). The formation of QOOH radicals is required for low-temperature chain-branching, which sustains oxidation and occurs via a second O_2-addition reaction QOOH + O_2 → OOQOOH [7]. However, competition for the formation of QOOH comes from both consumption reactions of R including product formation direct from (ROO → conjugate alkene + HO_2) and from chemical activation in R + O_2 reactions leading directly to bimolecular products. In addition, unimolecular decomposition reactions of QOOH compete with second O_2-addition and follow three types of reactions (Figure 1) that are either chain-inhibiting at low temperature, through the production of the relatively unreactive HO_2 radical, or chain-propagating via production of OH.

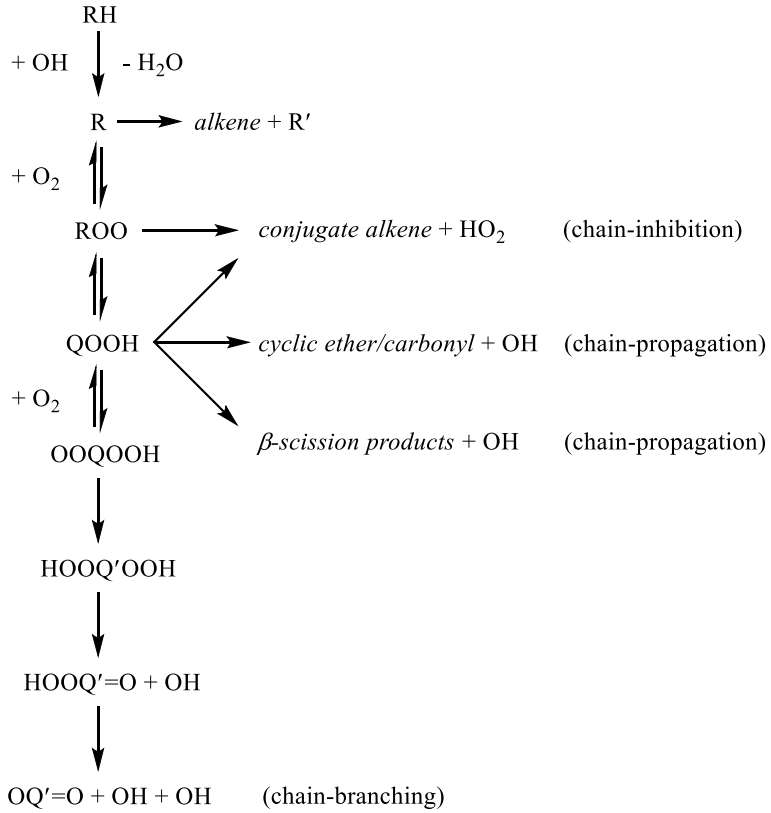

Figure 1. Alkane oxidation scheme.

The first of the three types of unimolecular QOOH decomposition leads to conjugate alkene + HO_2 (cf. Figure 1), occurring in β-QOOH isomers via C–O bond scission (Figure 2a), and is chain-inhibiting due to the formation of HO_2, which has an appreciably lower rate coefficient for the chain-propagating through H-abstraction from RH compared to OH [8]; ca. 10^4 at 700 K. However, H-abstraction reactions involving HO_2, subsequently forming H_2O_2, become more important towards ~ 800 K and are responsible for chain-branching in the intermediate temperature regime (i.e. the transition from low- to high-temperature), once the temperature is high enough for dissociation of H_2O_2 becomes significant. The second type of unimolecular decomposition of QOOH leads to cyclic ether or carbonyl species formed coincident with OH (cf. Figure 1), in a chain-propagation step. This decomposition involves concerted scission of the O–O in the hydroperoxy group yielding OH, and bond formation between the carbon-bound oxygen atom and the carbon with the unpaired electron (Figure 2b and Figure 2c). The co-product with OH depends on the C–O bond being formed, either with an α carbon – creating a ketone or an aldehyde (Figure 2b) – or with $\beta/\gamma/\delta/\varepsilon$ carbon, creating a cyclic ether (e.g. with β carbon, Figure 2c). The third type of unimolecular QOOH decomposition is a chain-propagation step involving concerted bond-scission, namely C–C β-scission, leading to alkene + carbonyl, and scission of the O–O bond in the hydroperoxy group, producing OH (Figure 2e). Collectively, the abovementioned reaction pathways compete with the consumption of QOOH radicals via QOOH + O_2 and thereby directly impact the landscape of chemical reactions involved in autoignition.

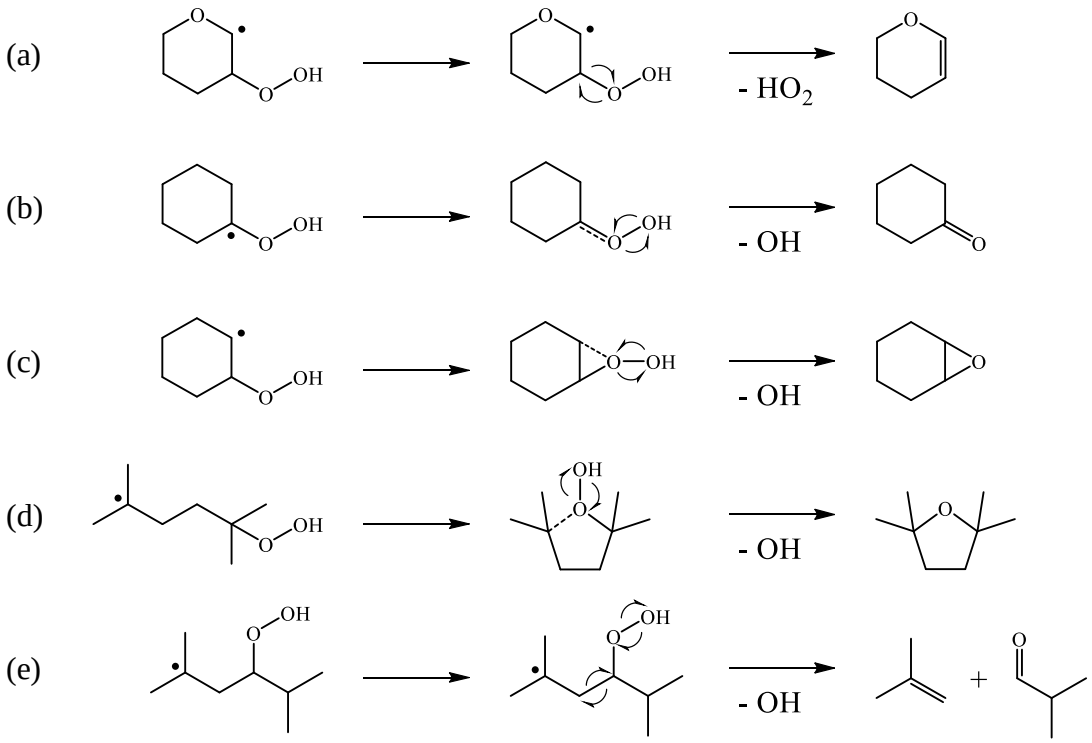

Figure 2. Unimolecular reactions of QOOH radicals. (a) Chain-termination step in tetrahydropyran oxidation, forming conjugate alkene (3,4-dihydro-*2H*-pyran). (b) – (e) Chain-propagation steps in cyclohexane oxidation via (b) α-QOOH, forming carbonyl (cyclohexanone) and (c) β-QOOH, forming cyclohexene oxide, and in 2,5-dimethylhexane oxidation via (d) δ-QOOH, forming cyclic ether (2,2,5,5-tetramethyltetrahydrofuran), and (e) γ-QOOH, forming methylpropanal + *iso*-butene.

In the development of comprehensive chemical kinetics models for hydrocarbons and oxygenated biofuels, reaction classes initially formulated around alkane oxidation [3] and alkene oxidation [9-11] are commonly adopted as starting points in the task of categorizing the types of reactions occurring in combustion systems. Rate rule analogies are often used as estimates where direct measurements or theoretical calculations are not available, or to modify alkane-based rate parameters to account for differences in molecular structure. Table 1 lists the types of reactions routinely included in the development of chemical kinetics models for alkanes. Alternative reaction pathways (not included in Table 1) were recently adopted that augment the alkane oxidation scheme in Figure 1 to include reactions starting from OOQOOH (i.e. third O_2-addition or HO_2-elimination from $HOOQ_{-H}OOH$) [12], initially postulated in Silke et al. [13].

Table 1. Reaction classes for alkane oxidation.

1	unimolecular decomposition of fuel	RH → products
2	H-abstraction from fuel	RH + X → R + HX
3	fuel radical decomposition	R → products
4	direct HO_2 formation	R + O_2 → conjugate alkene + HO_2
5	fuel radical isomerization	R → R′
6	abstraction from conjugate alkene	conjugate alkene + X → alkenyl + HX
7	radical addition to conjugate alkenes	conjugate alkene + X → adduct
8	alkenyl radical decomposition	alkenyl → products
9	conjugate alkene decomposition	R_{-H} → products
10	O_2-addition to initial fuel radical	R + O_2 → ROO
11	fuel radical-peroxy radical disproportionation	R + R′OO → RO + R′O
12	hydroperoxyalkyl radical formation via peroxy radical isomerization	ROO → QOOH
13	hydroperoxide formation via HO_2	ROO + HO_2 → ROOH + O_2
14	hydroperoxide formation via H_2O_2	ROO + H_2O_2 → ROOH + HO_2
15	alkoxy radical formation	ROO + H_3COO → RO + H_3CO + O_2
16	peroxy + peroxy	ROO + R′OO → RO + R′O + O_2
17	alkoxy formation via unimolecular decomposition of organic hydroperoxide	ROOH → RO + OH
18	unimolecular alkoxy radical decomposition	RO → products
19	unimolecular QOOH decomposition into cyclic ether + OH (ring closure via concerted O–O scission and C–O bond formation)	QOOH → cyclic ether + OH
20	unimolecular QOOH decomposition into conjugate alkene + HO_2 (C–O bond scission)	β-QOOH → conjugate alkene + HO_2
21	unimolecular QOOH decomposition into carbonyl (ketone/aldehyde) + alkene + OH (concerted C–C scission and C–O bond scission)	QOOH → carbonyl + alkene + OH
22	O_2-addition to QOOH	QOOH + O_2 → OOQOOH
23	isomerization of OOQOOH into KHP	OOQOOH → $HOOQ_{-H}OOH$
24	decomposition of ketohydroperoxide	$HOOQ_{-H}OOH$ → $HOOQ_{-H}O$ + OH
25	cyclic ether reactions	cyclic ether + OH/HO_2 → products

1.1. Chemical Kinetics Models

Three comprehensive chemical kinetics models were selected from the literature to examine the level of detail paid to describing low-temperature chemistry of primary oxidation intermediates, defined herein as species formed in initial R + O_2 reactions of parent molecules: the 2,5-dimethylhexane model of Sarathy et al. [14], 883 species and 4204 reactions, and the cyclohexane models of Silke et al. [13], 1081 species and 4269 reactions, and Serinyel et al. [15], 375 species and 1344 reactions. Relevant rate coefficients from these models were extracted and tabulated in the Appendix.

1.2. Comparison of Primary Oxidation Intermediate Concentrations

The perfectly stirred reactor (PSR) module in ChemKin v17.2 was employed to calculate species mole fractions in dilute (99% Ar), stoichiometric oxidation of 2,5-dimethylhexane, using Sarathy et al. [14], and cyclohexane using Silke et al. [13] and Serinyel et al. [15]. Residence time and pressure were fixed at 2 s and 10 atm, respectively. In all cases the steady state solver was used in conjunction with fixed gas temperature for the solution steps, which were carried out in increments of 10 K from 500 – 1000 K. Initial mole fractions for 2,5-dimethylhexane oxidation were RH = $0.07 \cdot 10^{-2}$, $O_2 = 0.93 \cdot 10^{-2}$, and Ar = 0.99 and for cyclohexane, RH = $0.10 \cdot 10^{-2}$, $O_2 = 0.90 \cdot 10^{-2}$, and Ar = 0.99. Mole fraction ratios, defined as the ratio of the parent molecule (e.g. 2,5-dimethylhexane) relative to a primary oxidation intermediate (e.g. 2,2,5,5-tetramethyl-tetrahydrofuran), were calculated to assess relative concentrations as a function of temperature.

Mole fraction calculations of 2,5-dimethylhexane and several primary oxidation intermediates using the model of Sarathy et al. [14] are shown in Figure 3a. Negative temperature dependence is evident from ca. 600 – 750 K, in both 2,5-dimethylhexane and the cyclic ether 2,2,5,5-tetramethyltetrahydrofuran. Formation of 2,5-dimethylhexene isomers becomes important near 650 K, yet remains minor relative to the production of the cyclic ether. Figure 3b shows mole fraction ratios calculated for 2,2,5,5-tetramethyltetrahydrofuan and the three 2,5-dimethylhexene isomers. The most relevant result in Figure 3b is the mole fraction ratio for the cyclic ether, which is < 10:1 from approximately 550 – 850 K, which suggests that it could compete with the parent molecule for OH and other radicals, i.e. both OH + RH and OH + intermediate reactions become relevant under such conditions.

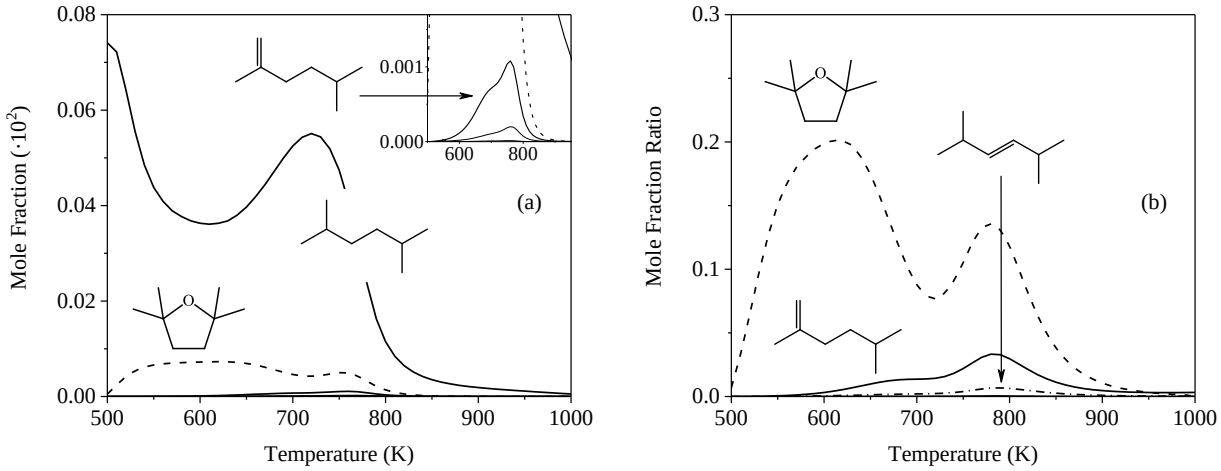

Figure 3. (a) Temperature dependence of mole fractions calculated from stoichiometric 2,5-dimethylhexane oxidation at 10 atm and residence time of 2 s using the model of Sarathy et al. [14] in the PSR module of ChemKin v17.2. (b) Mole fraction ratios of primary oxidation intermediates relative to 2,5-dimethylhexane calculated using the results in (a). The mole fraction ratio of 2,2,5,5-tetramethyltetrahydrofuran being > 0.1 for most temperatures suggests competition with the parent molecule, 2,5-dimethylhexane, for OH and other radicals. Initial mole fractions: 2,5-dimethylhexane = $0.07 \cdot 10^{-2}$, $O_2 = 0.93 \cdot 10^{-2}$, and Ar = 0.99.

Mole fractions calculated for cyclohexane oxidation using the Silke et al. [13] model are shown in Figure 4a, where negative temperature dependence is observed from ca. 625 – 750 K. Cyclohexene is the dominant primary oxidation intermediate formed, with the mole fractions for 1,2-epoxycyclohexane and 1,4-epoxycyclohexane (not shown) being approximately 10 times lower. Mole fraction ratios calculated for cyclohexene and 1,2-epoxycyclohexane using the model of Silke et al. [13] yield results similar to 2,5-dimethylhexane (cf. Figure 3). The mole fraction ratio in Figure 4b of cyclohexene relative to cyclohexane is higher than 0.1 for most temperatures, which raises the question of the importance of including R + O_2 chemistry for primary oxidation intermediates in chemical kinetics models. In addition, note that cyclohexene oxide (1,2-epxoycyclohexane) is underpredicted in both models, by up to a factor of five at both dilute conditions [15] and non-dilute conditions [13], the results in Figure 4b may represent lower limits.

The simulations therefore suggest that subsequent oxidation of the intermediate products from the primary oxidation step could play a role in the ignition chemistry of cyclohexane and 2,5-dimethylhexane. In the ensuing sections, the fundamental oxidation reactions of these intermediates is examined.

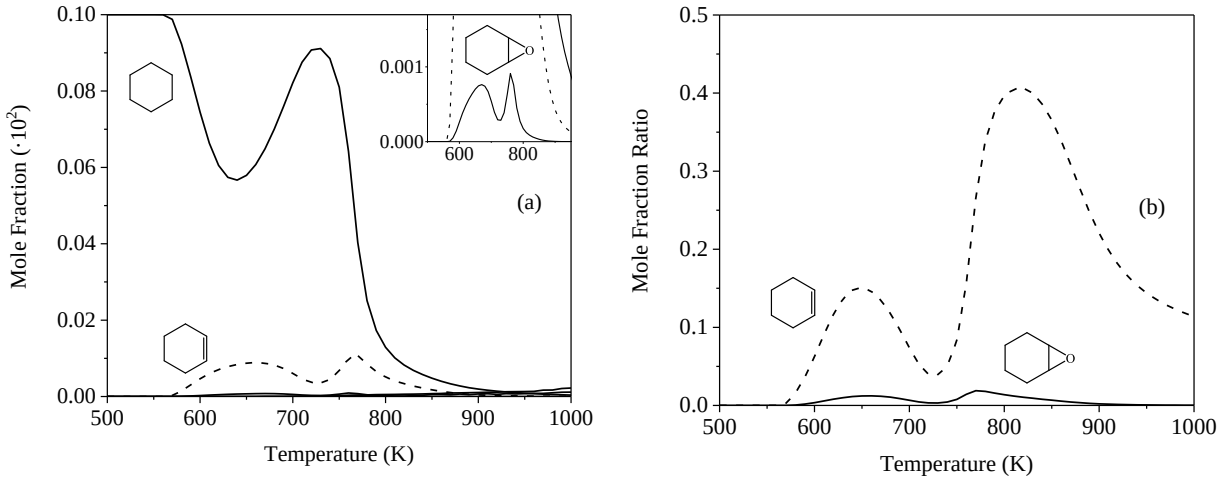

Figure 4. (a) Temperature dependence of mole fractions calculated from stoichiometric cyclohexane oxidation at 10 atm and residence time of 2 s using the model of Silke et al. [13] in the PSR module of ChemKin v17.2. (b) Mole fraction ratios of primary oxidation intermediates relative to cyclohexane calculated using the results in (a). The mole fraction ratio of cyclohexene being > 0.1 for most temperatures suggests competition with the parent molecule, cyclohexane, for OH and other radicals. Initial mole fractions: cyclohexene = $0.1 \cdot 10^{-2}$, $O_2 = 0.9 \cdot 10^{-2}$, and Ar = 0.99.

2. EXPERIMENTAL APPROACH

Time-dependent mass spectra of product formation from Cl-initiated oxidation of alkene and cyclic ether species were measured at 700 K and 10 Torr using multiplexed photoionization mass spectrometry (MPIMS). The species selected for the experiments were 2,5-dimethylhex-1-ene, 2,5-dimethylhex-2-ene, 2,5-dimethylhex-3-ene, 2,2,5,5-tetramethyltetrahydrofuran, cyclohexene, cyclohexene oxide, 3,4-dihydro-*2H*-pyran, and 3,6-dihydro-*2H*-pyran (Table 2), which are primary oxidation intermediates detected in prior studies of 2,5-dimethylhexane [16] and cyclohexane and tetrahydropyran [17]. Other primary oxidation intermediates were also detected, e.g. methylpropanal, 3-butenal, *iso*-butene, propene, formaldehyde, however the focus of the experiments herein is on alkenes formed coincident with HO_2 directly from parent molecules and cyclic ethers formed via unimolecular QOOH decomposition.

Table 2. Intermediates formed from initial R + O_2 reactions in the oxidation of several species (RH): 2,5-dimethylhexane, cyclohexane, and tetrahydropyran.

RH	intermediates formed from R + O_2 reactions
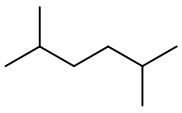	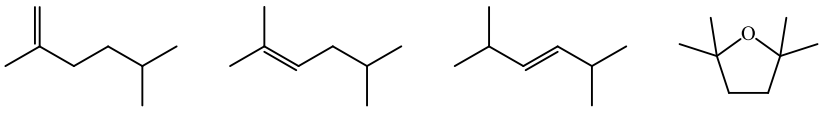
	
	

The MPIMS experiments were conducted in a 1.05-cm diameter slow-flow quartz reactor [18] using pulsed-photolytic chlorine atom-initiated oxidation, highly diluted in He, with constant initial reactant number densities (Table 3). Photolysis of either molecular chlorine (Cl_2), using unfocused 351-nm light from an excimer laser, or oxalyl chloride, $(COCl)_2$, using unfocused 248-nm light from an excimer laser, generated Cl atoms homogeneously along both the radial and longitudinal axes of the reactor. The Cl atoms abstract H atoms via RH + Cl → R + HCl under pseudo-first-order conditions (such that [RH] >> [Cl]) to form the initial R radicals, which subsequently undergo pseudo-first-order reaction with O_2. No determination of the distribution of initial R radicals is made herein. However, structure activity relations (SAR) based on the work of Atkinson [19] for RH + Cl → R + HCl were used in the initial studies on 2,5-dimethylhexane [16] and cyclohexane and tetrahydropyran [17]. To minimize side chemistry unrelated to R + O_2, pseudo-first-order conditions were employed for RH + Cl such that R + Cl reactions remain negligible, and the > 10^3 excess of [O_2] relative to [Cl] forces R + O_2 to be the dominant reaction.

Figure 5. Multiplexed photoionization mass spectrometer [18].

Table 3. Initial number densities of reactants (molecules · cm^{-3}) and pressures used for Cl-initiated oxidation experiments on tetrahydropyran and cyclohexane. [He] dilution balance is not listed. Pseudo-first-order conditions were used. $[RH]_0$:$[Cl]_0$ > 20 and $[O_2]_0$:$[R]_0$ > 2000.

pressure	$[RH]_0$	$[O_2]_0$	$[Cl]_0$
10 Torr	$1.9 \cdot 10^{14}$	$1.9 \cdot 10^{16}$	$8.8 \cdot 10^{12}$

The generation of Cl atoms from 248-nm photolysis of oxalyl chloride ($\sigma_{248\ nm}$ = 2.66 10^{-19} cm^2 molec.$^{-1}$ [20, 21]) occurs via a single-photon process and a two-step mechanism [20]. The first Cl atom is generated instantaneously with a quantum yield of one by $(COCl)_2 + h\nu \rightarrow Cl + CO + ClCO^*$, and the second Cl atom is generated from dissociation of chemically activated ClCO via $ClCO^* \rightarrow Cl + CO$ on timescales appreciably short relative to the oxidation timescales of interest. Under the experimental conditions herein, collisional quenching of ClCO* is unimportant (i.e. the ClCO* dissociation rate is shorter than the time between collisions) and the timescale of the second step is ~ 1 μs [20]. The co-product of $(COCl)_2$ photolysis, CO, is unreactive at the temperatures and pressures herein and is not relevant to the oxidation reactions studied. Depletion timescales of Cl by RH under the concentrations listed in Table 1 are ~ 20 μs at 10 Torr and ~ 1 μs at 1500 Torr, assuming $k_{RH + Cl}$ ~ 10^{-10} cm^3 · molec.$^{-1}$ · s^{-1}.

The photoionization experiments were conducted at both Sandia National Laboratories, using the Lyman-alpha line of a hydrogen discharge lamp (nominal photon energy of 10.2 eV, with a range of 8.5 – 10.3 eV) and the Chemical Dynamics Beamline of the Advanced Light Source [22, 23] at 11.0 eV. Products from the Cl-initiated oxidation reactions exit the quartz reactor through a 600-μm side orifice into a detector region maintained at ~ 10^{-8} Torr forming a near-effusive molecular beam, which is then collimated by a 1.5-mm diameter skimmer positioned approximately 2 mm downstream from the side orifice. Cations, consisting of both parent and fragment ions, are formed by orthogonally intersecting the collimated molecular beam with a (quasi-) continuous beam of VUV photons and then detected using an orthogonal-acceleration time-of-flight mass spectrometer equipped with microchannel plates.

Photoionization mass spectra were recorded at 20-μs time intervals over a span of 150 ms (20-ms pre-photolysis and 130-ms post-photolysis). The time-dependent mass spectra were measured using a 4-Hz photolysis repetition rate of the excimer laser and signal-averaging of approximately 10^4 laser shots. In order to ensure that no residual gases from the previous reaction remained, flow rates were set such that the volume inside of the reactor was completely replenished with reactants in between laser pulses, a process verified by observing a baseline pre-photolysis signal of zero for *m/z* corresponding to product masses. Background-subtraction is applied to the mass spectra to remove non-time-resolved pre-photolysis signals, producing difference mass spectra. Time-dependent measurements of ion signal, $S_i(E)$, for both *m/z* are extracted from the mass spectra, where $S_i(E)$ is defined by Equation 1 by an energy and mass-independent instrument factor, Λ, absolute photoionization cross-section, $\sigma_i(E)$, species concentration, c_i, species mass, m_i, and a mass discrimination factor, $\beta(P,T)$. The latter factor is measured in separate experiments.

$$S_i(E) = \Lambda\, \sigma_i(E) c_i\, m_i^{\beta(P,T)} \qquad (1)$$

3. RESULTS

The sections below present mass spectra and time profiles measured in Cl-initiated oxidation experiments of alkene and cyclic ether intermediates derived from R + O_2 reactions of 2,5-dimethylhexane (Section 3.1), cyclohexane (Section 3.2), and tetrahydropyran (Section 3.3). The focus of the analysis is on mass peaks that relate directly to products from either direct ROO decomposition into conjugate alkene + HO_2 or to products of QOOH-mediated pathways, namely *m/z* that correspond to conjugate alkene (parent *m/z* – 2 amu) and cyclic ether/carbonyl (parent *m/z* + 14 amu). The ensuing results report only ion signal and therefore no quantification of any species is conducted, which requires absolute photoionization cross-sections via Equation 1. However, the main results and conclusions rest on the detection of time-dependent ion signal at *m/z* that correspond to either conjugate alkene or cyclic ether/carbonyl species, which serve as indicators of preceding QOOH formation. In the former case, direct formation from ROO does not involve the formation of QOOH, and likely contributes partially to the measured alkene yield. However, thermalized, QOOH-mediated pathways become increasingly important with temperature and given the 700 K experiments herein are expected to be the dominant conjugate alkene + HO_2 pathway.

3.1. Product Formation from R + O_2 Reactions of Intermediates Formed in 2,5-dimethylhexane Oxidation

The MPIMS measurements in Rotavera et al. [16], conducted at conditions similar to the present experiments (10 Torr and 550 K and 650 K), identified all four intermediates in Table 2 as significant products of R + O_2 reactions in 2,5-dimethylhexane. The cyclic ether in Table 2, 2,2,5,5-tetramethyltetrahydrofuran, is derived only from (tertiary) 2,5-dimethylhex-2-yl radicals and results from a sequence of reactions that is facilitated by an energetically favorable 7-membered transition state in the ROO → QOOH isomerization step, and from the lower C–H bond energy of the transferred tertiary hydrogen. In addition, the pathway, which is mediated by a tertiary-tertiary QOOH radical, is enhanced by facile primary → tertiary alkyl radical isomerization reactions providing an additional source of tertiary R. The conditions leading to the formation of 2,2,5,5-tetramethyltetrahydrofuran are expected to be enhanced in OH-initiated systems given the higher selectivity of OH compared to chlorine atoms, and therefore a higher propensity to form tertiary radicals. The favorable kinetics leading to the formation of 2,2,5,5-tetramethyltetrahydrofuran emphasizes the relevance of examining the low-temperature chemistry of the cyclic ether initiated by R + O_2 reactions. Similarly, given the positive temperature dependence associated with R + O_2 → conjugate alkene + HO_2 in alkane oxidation, the 2,5-dimethylhexene isomers are expected to be of considerable importance above ca. 600 K as evidenced by the jet-stirred reactor results in Sarathy et al. [14] and all three isomers were quantitatively significant in Rotavera et al. [16].

Product formation from reaction of 2,5-dimethylhexen-yl isomers with O_2 follows, in part, the oxidation paradigm in Figure 1 with additional reactions likely involved, including radical-addition to unsaturated carbon, retroene reactions, and others. Alkene-specific reactions augmenting Figure 1 that account for unsaturated carbon are discussed in studies on hexene isomers, e.g. Mehl et al. [9], Bounaceur et al. [10], and Battin-Leclerc et al. [11]. Reactions of O_2

with either of the two types of radicals of 2,2,5,5-tetramethyltetrahydrofuran are expected to exhibit similarity with the alkane sequence in Figure 1, due to the absence of sp^2 carbon, although the presence of an ether group promotes ring-opening reactions in initial radicals, which competes with O_2-addition and subsequent ROO or QOOH formation [17].

3.1.1. 2,5-dimethylhex-1-ene

Initiation reactions via H-abstraction in 2,5-dimethylhex-1-ene oxidation lead to five distinct initial radicals (Figure 6): two primary radicals (Figure 6a and 6e), two secondary radicals (Figure 6c and 6d), and one tertiary radical (Figure 6b). Resonance-stabilized radicals are formed in abstraction reactions involving allylic H atoms on both primary and secondary carbon atoms, Figures 6e and 6d, respectively. Well-depths for peroxy adducts in which the initial R radicals are saturated alkyl species are expected to be approximately 35 kcal/mol with respect to the R + O_2 reactants, while peroxy adducts from O_2-addition to resonance-stabilized radicals are higher in energy relative to this by approximate 15 kcal/mol. Shallower ROO well-depths disfavor isomerization reactions that lie above the R + O_2 entrance channel, favoring instead back dissociation to reactants. In both cases, however, the formation of both cyclic ethers and carbonyl (i.e. parent *m/z* + 14) and conjugate alkenes (i.e. parent *m/z* – 2) are possible. The nominal mass-to-charge ratio of 2,5-dimethylhex-1-ene is *m/z* = 112.

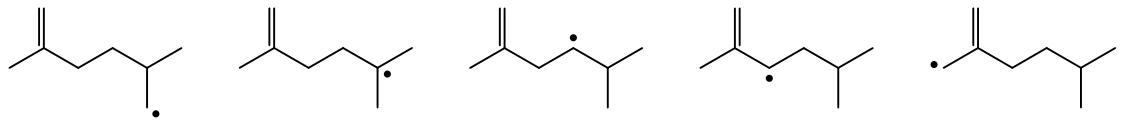

(a) (b) (c) (d) (e)

Figure 6. Initial R radicals formed in H-abstraction reactions of 2,5-dimethylhex-1-ene. Vinylic radicals are not depicted due to expected low yield from RH + Cl given the higher barrier to abstraction relative to alkylic sites [24, 25]).

Figure 7 shows the background-subtracted photoionization mass spectrum of product species formed in Cl-initiated oxidation of 2,5-dimethylhex-1-ene. The mass-to-charge ratios of primary oxidation products, formed directly from R + O_2 reactions, include *m/z* = 110 and *m/z* = 126, which correspond to conjugate alkene + HO_2 and cyclic ether/carbonyl + OH channels respectively. Other products include *m/z* = 42 (propene or ketene) and *m/z* = 68 (isoprene), which may form via QOOH decomposition. Ion signal in Figure 7 at *m/z* = 108 indicates further oxidation of the *m/z* 110 species via HO_2-elimination. Time profiles were extracted from the background-subtracted mass spectra for *m/z* = 110 and *m/z* = 126 (Figure 8). The *m/z* = 110 time profile is composed of contributions from direct and sequential HO_2 formation mechanisms, the latter signifying the formation of QOOH radicals. Similarly, the time-dependent signal at *m/z* = 126 also signifies the formation of QOOH radicals. Although reference absolute or relative photoionization spectra are required to identify the molecular structure of the specific C_8H_{14} and $C_8H_{14}O$ isomers, the detection of time-resolved *m/z* = 110 and *m/z* = 126 ion signals on primary timescales confirm that 2,5-dimethylhex-1-ene, an intermediate oxidation product of 2,5-dimethylhexane oxidation,

proceeds through pathways similar to Figure 1 by forming QOOH radicals that subsequently undergo unimolecular decomposition to form conjugate alkene and cyclic ether/carbonyl species.

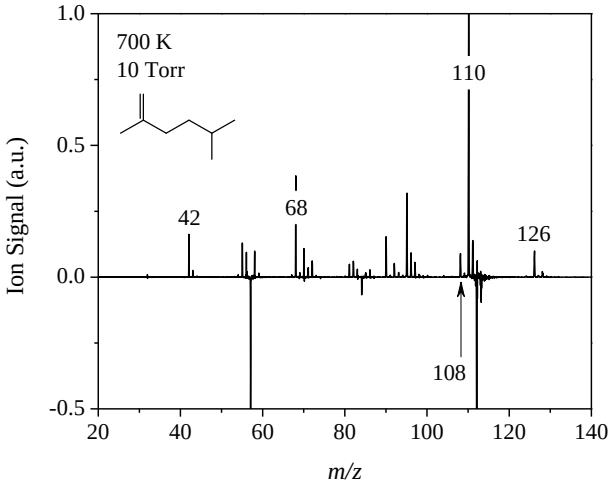

Figure 7. Difference mass spectrum of Cl-initiated oxidation of 2,5-dimethylhex-1-ene (*m/z* = 112); 700 K, 10 Torr. Negative ion signal indicates pre-photolysis photoionization of 2,5-dimethylhex-1-ene.

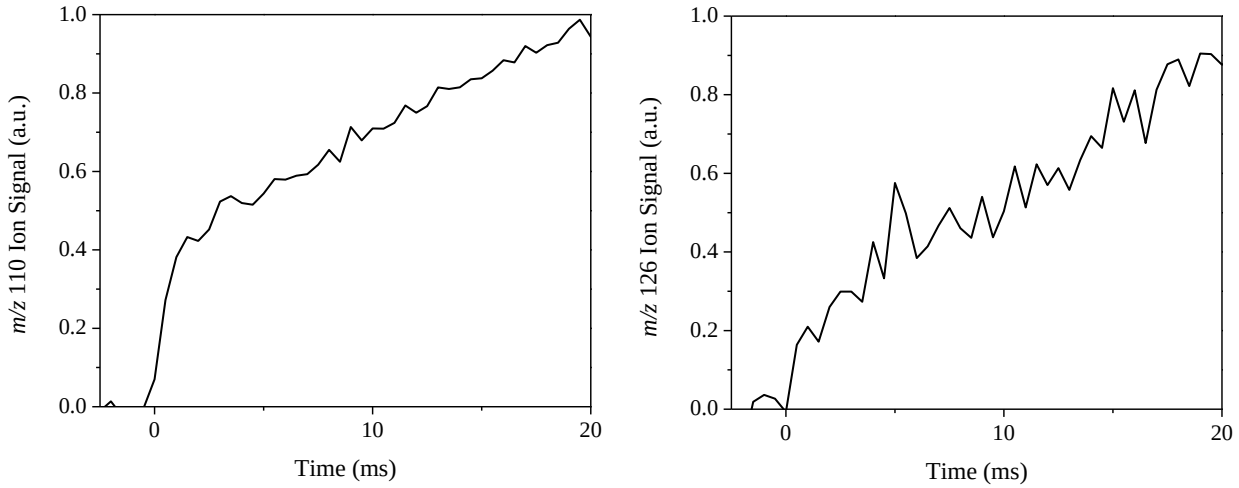

Figure 8. Time profiles of *m/z* = 110 (conjugate alkene) and *m/z* = 126 (cyclic ether / carbonyl) formed from oxidation of 2,5-dimethylhex-1-en-yl radicals.

Considering the asymmetric molecular structure of 2,5-dimethylhex-1-ene, the R + O_2 potential energy surfaces for alkenyl isomers contain a large number of chain-propagating and chain-terminating reactions. The total number of reactions leading to *m/z* = 110 conjugate alkenes, including both direct and sequential pathways, is 12, and the total number of QOOH-mediated reactions leading to *m/z* = 126, either cyclic ether or carbonyl species formed coincident with OH, is 25. Computation of the barrier heights are outside the scope of the present work. However, representative reactions leading to *m/z* = 110 conjugate alkene + HO_2 and *m/z* = 126 cyclic ether + OH are depicted in Figure 9.

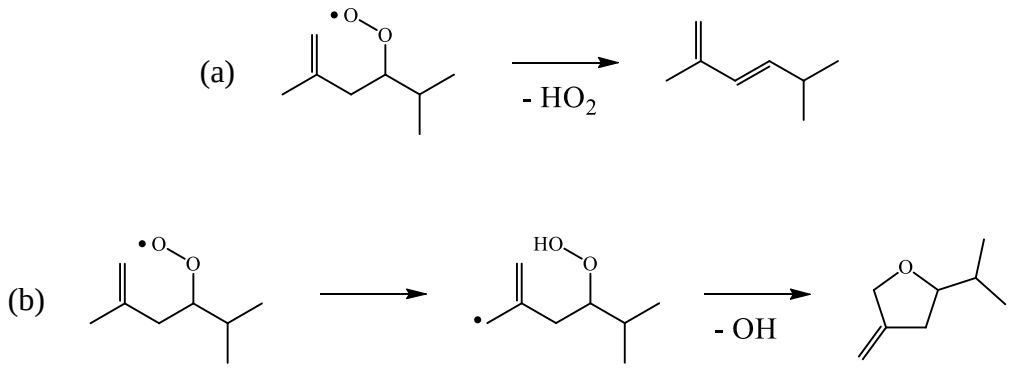

Figure 9. Representative reaction sequences of 2,5-dimethylhex-1-en-4-peroxy radicals leading to (a) 2,5-dimethyl-1,4-hexadiene (*m/z* = 110) + HO_2 and (b) 2-*iso*-propyl-4-methylene-tetrahydrofuran (*m/z* = 126) + OH.

R + O_2 chemistry for 2,5-dimethylhex-1-ene, where R represents one of the five 2,5-dimethylhex-1-en-yl radical isomers in Figure 6 and that leads to the representative species in Figure 9, is not included for 2,5-dimethylhex-1-ene in the model of Sarathy et al. [14]. Formation reactions in [14] leading to 2,5-dimethylhex-1-ene (Appendix, Table A1) include C–H β-scission in alkenyl radicals, direct formation via 2,5-dimethylhex-1- and -2-yl-peroxy radicals, and C–O bond-scission in β-QOOH radicals. The types of consumption reactions for 2,5-dimethylhex-1-ene in [14], written in the forward direction, include: (1) abstraction reactions with OH/HO_2/H/CH_3/O yielding a single *lumped* species representing all 2,5-dimethylhex-*A*-en-*B*-yl radical isomers (Where A is the location of the C=C bond and B is the location of the carbon atom with the unpaired electron), (2) disproportionation reactions with OH/O, and (3) homolysis reactions. The)(lumped) alkenyl radicals produced via H-abstraction from 2,5-dimethylhex-1-ene are prescribed only to undergo subsequent reaction with HO_2, methoxy (H_3CO), and ethoxy (H_3CCH_2O) and C–C β-scission reactions. Reactions of the lumped radical with O_2 are neglected.

3.1.2. 2,5-dimethylhex-2-ene

Initiation reactions via H-abstraction in 2,5-dimethylhex-2-ene oxidation lead to four distinct initial radicals (Figure 10): two primary radicals (Figures 10a and 10d), one secondary radical (Figures 10c), and one tertiary radical (Figures 10b). Similar to 2,5-dimethylhex-1-ene, resonance-stabilized radicals are formed from abstraction reactions involving allylic H atoms on both primary and secondary carbon atoms, Figures 10d and 10c respectively. One difference presented with the shift in the location of the double bond in 2,5-dimethylhex-2-ene is the reduction in size of the aliphatic portion of the molecule, from *iso*-pentyl to *iso*-butyl, which affects the number of favorable pathways on the various R + O_2 potential energy surfaces. In particular, transition states leading to 5-membered cyclic ethers (oxolanes) requires abstraction of vinylic hydrogen, while the formation of 6-membered cyclic ethers (oxanes) are not possible given the absence of hydrogen atoms on the corresponding sp^2-hybridized tertiary carbon. In addition, given the higher number of H-abstraction sites from primary carbon adjacent to the C=C bond and accounting for the adjacent secondary allylic hydrogen, the number of possible resonance-stabilized initial radicals is

increased in 2,5-dimethylhex-2-ene compared to 2,5-dimethylhex-1-ene, where the terminal carbon is sp^2-hybridized. Accordingly, the probability for ROO well-depths that disfavor ROO → QOOH isomerization reactions, favoring instead back dissociation to R + O_2 reactants, increases. Despite the effect of the location of the C=C bond, formation of both cyclic ethers and carbonyl (i.e. parent *m/z* + 14) and conjugate alkenes (i.e. parent *m/z* – 2) remains plausible. The nominal mass-to-charge ratio of 2,5-dimethylhex-2-ene is *m/z* = 112.

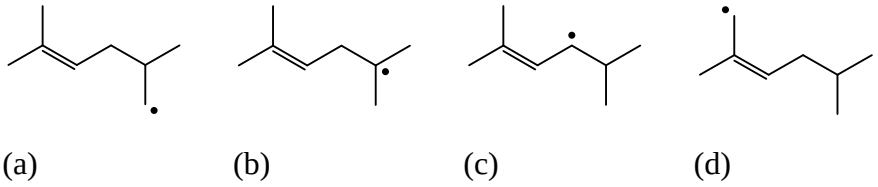

Figure 10. Initial R radicals formed in H-abstraction reactions of 2,5-dimethylhex-2-ene (vinylic radicals not depicted due to expected low yield from RH + Cl given the higher barrier to abstraction relative to alkylic sites [24, 25]).

Figure 11 shows the background-subtracted photoionization mass spectrum of product species formed in Cl-initiated oxidation of 2,5-dimethylhex-2-ene. The mass-to-charge ratios of primary oxidation products, formed directly from R + O_2 reactions, include *m/z* = 110 and *m/z* = 126, which correspond to conjugate alkene + HO_2 and cyclic ether/carbonyl + OH channels respectively. Other products include *m/z* = 42 (propene or ketene) and *m/z* = 68 (isoprene), similar to 2,5-dimethylhex-1-ene and which may form via QOOH decomposition. *m/z* = 58, i.e. *iso*-butene (C_4H_8) or acetone (C_3H_6O), is also evident, with the former arising from β-scission of the tertiary radical 2,5-dimethylhex-2-en-5-yl. Time profiles were extracted from the background-subtracted mass spectra for *m/z* = 110 and *m/z* = 126 (Figure 12). The *m/z* = 110 time profile is composed of contributions from both direct and sequential HO_2 formation mechanisms, the latter signifying the formation of QOOH radicals. Similarly, the time-dependent signal at *m/z* = 126 also signifies the formation of QOOH radicals. Although reference absolute or relative photoionization spectra are required to identify the molecular structure of the specific C_8H_{14} and $C_8H_{14}O$ isomers, the detection of time-resolved *m/z* = 110 and *m/z* = 126 ion signals on primary timescales confirm that 2,5-dimethylhex-2-ene, an intermediate oxidation product of 2,5-dimethylhexane oxidation, proceeds through pathways similar to Figure 1 by forming QOOH radicals that subsequently undergo unimolecular decomposition to form conjugate alkene and cyclic ether/carbonyl species.

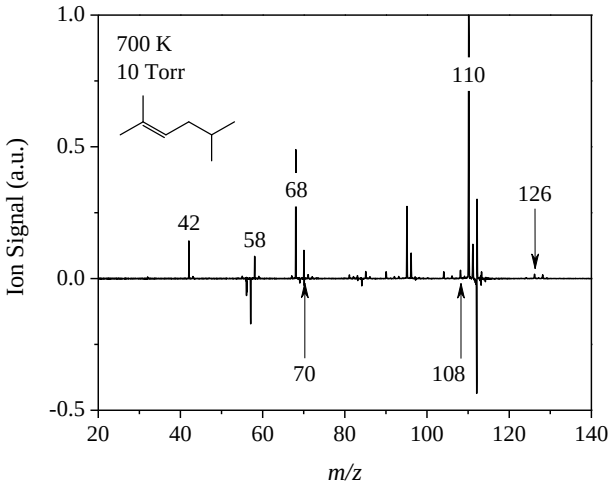

Figure 11. Difference mass spectrum of Cl-initiated oxidation of 2,5-dimethylhex-2-ene (*m/z* = 112); 700 K, 10 Torr. Negative ion signal indicates pre-photolysis photoionization of 2,5-dimethylhex-2-ene.

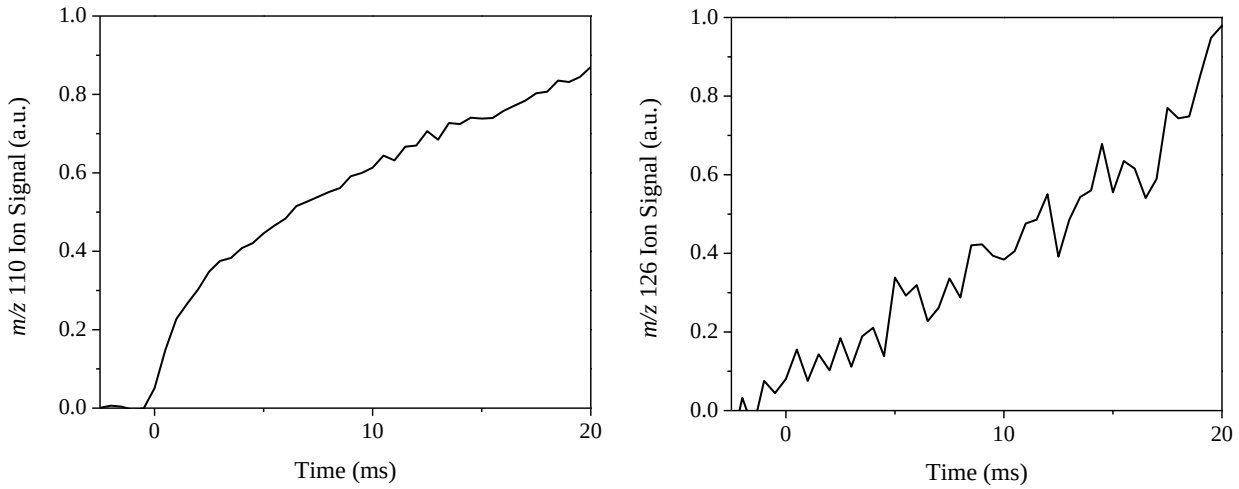

Figure 12. Time profiles of *m/z* = 110 (conjugate alkene) and *m/z* = 126 (cyclic ether / carbonyl) formed from oxidation of 2,5-dimethylhex-2-en-yl radicals.

Considering the asymmetric molecular structure of 2,5-dimethylhex-2-ene, similar to 2,5-dimethylhex-1-ene, the R + O_2 potential energy surfaces for alkenyl isomers contain a large number of chain-propagating and chain-terminating reactions. The total number of reactions leading to *m/z* = 110 conjugate alkenes, including both direct and sequential pathways, is 8, and the total number of QOOH-mediated reactions leading to *m/z* = 126, either cyclic ether or carbonyl species formed coincident with OH, is 17. Representative reactions leading to *m/z* = 110 conjugate alkene + HO_2 and *m/z* = 126 cyclic ether + OH are depicted in Figure 13.

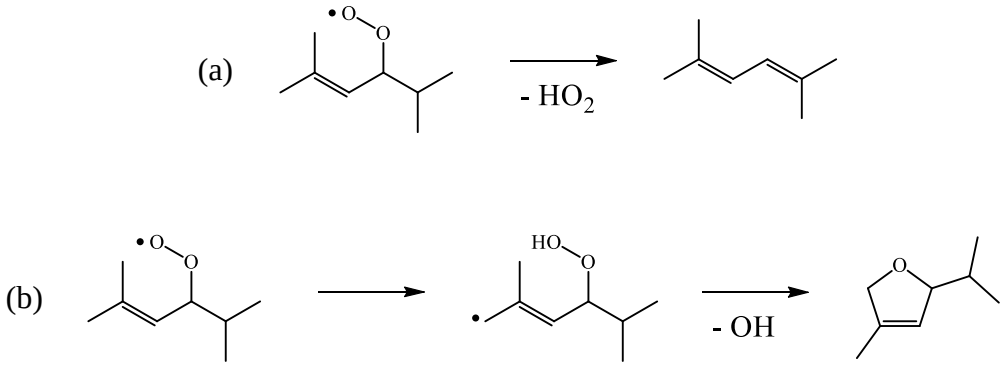

Figure 13. Representative reaction sequences of 2,5-dimethylhex-2-en-4-peroxy radicals leading to (a) 2,5-dimethyl-2,4-hexadiene (*m/z* = 110) + HO_2 and (b) 2-*iso*-propyl-4-methyl-5H-furan (*m/z* = 126) + OH.

R + O_2 chemistry, where R represents one of the four 2,5-dimethylhex-2-en-yl radical isomers in Figure 10 and that leads to the representative species in Figure 13, is not included for 2,5-dimethylhex-2-ene in the model of Sarathy et al. [14] model. Formation reactions in [14] leading to 2,5-dimethylhex-2-ene (Appendix, Table A2) include C–H β-scission in alkenyl radicals, direct formation via 2,5-dimethylhex-2- and -3-yl-peroxy radicals, and C–O bond-scission in β-QOOH radicals. The types of consumption reactions for 2,5-dimethylhex-2-ene in [14], written in the forward direction, are similar to reactions consuming 2,5-dimethylhex-1-ene and include: (1) abstraction reactions with OH/HO_2/H/CH_3/O yielding a single *lumped* species representing all 2,5-dimethylhex-*A*-en-*B*-yl radical isomers, (2) disproportionation reactions with OH/O, and (3) homolysis reactions. The (lumped) alkenyl radicals produced via H-abstraction from 2,5-dimethylhex-2-ene are only prescribed to undergo subsequent reaction with HO_2, methoxy (H_3CO), and ethoxy (H_3CCH_2O) and C–C β-scission reactions.

3.1.3. 2,5-dimethylhex-3-ene

Initiation reactions via H-abstraction in 2,5-dimethylhex-3-ene oxidation leads only to two distinct initial radicals (Figure 14): one primary radical (Figure 15a) and one tertiary radical (Figure 15b). The shift in the location of the C=C bond in 2,5-dimethylhex-3-ene – compared to the location in the other two isomers – is a reduction in size of the aliphatic portion of the molecule to *iso*-propyl, which further reduces the number of favorable pathways on the various R + O_2 potential energy surfaces, evident by noting that isomerization reactions of primary ROO → QOOH via 6- and 7-membered transition states that involve secondary carbon both require abstraction of vinylic H atoms. An alternative pathway involving a 6-membered transition state exists, creating a primary-primary QOOH, where both the –OOH group and the unpaired electron are on primary carbon, the decomposition of which leads to a substituted oxetane species. However, the energy barriers for such pathways are commonly above the energy of the R + O_2 entrance channel. The remaining isomerization pathways of primary ROO radicals of 2,5-dimethylhex-3-ene involve either energetically or entropically disfavored pathways: (1) substituted oxirane via decomposition of a QOOH formed from a 5-membered ROO → QOOH transition state within which tertiary allylic hydrogen is abstracted and results in a resonance-stabilized QOOH, or (2) substituted oxane, which

is derived from an 8-membered transition state. Despite the effect of the location of the C=C bond and the reduction of favorable ROO → QOOH isomerization pathways, formation of both cyclic ethers / carbonyl (i.e. parent *m/z* + 14) and conjugate alkenes (i.e. parent *m/z* – 2) remains plausible. The nominal mass-to-charge ratio of 2,5-dimethylhex-2-ene is *m/z* = 112.

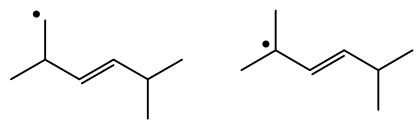

(a) (b)

Figure 14. Initial R radicals formed in H-abstraction reactions of 2,5-dimethylhex-3-ene (vinylic radicals not depicted due to expected low yield from RH + Cl given the higher barrier to abstraction relative to alkylic sites [24, 25]).

Figure 15 shows the background-subtracted photoionization mass spectrum of product species formed in Cl-initiated oxidation of 2,5-dimethylhex-3-ene. The mass-to-charge ratios of primary oxidation products, formed directly from R + O_2 reactions, include *m/z* = 110 and *m/z* = 126, which correspond with conjugate alkene + HO_2 and cyclic ether/carbonyl + OH channels respectively. However, the main mass peak evident in Figure 15 is *m/z* = 110, which is 2,5-dimethyl-1,4-hexadiene. No other significant mass peaks exist, with the exception of *m/z* = 42 (propene or ketene) and *m/z* = 95, which exhibits a stable time profile indicating that the mass peak arises from photofragmentation of an unknown species. The reduction in the number of products (i.e. mass peaks) in the mass spectrum of 2,5-dimetylhex-3-ene is consistent with the restriction of the number of favorable ROO → QOOH isomerization pathways.

Time profiles were extracted from the background-subtracted mass spectra for *m/z* = 110 and *m/z* = 126 (Figure 16). The *m/z* = 110 time profile is composed of contributions from both direct and sequential HO_2 formation mechanisms, the latter signifying the formation of QOOH radicals. Similarly, the time-dependent signal at *m/z* = 126 also signifies the formation of QOOH radicals. However, in contrast to 2,5-dimethylhex-1- and -2-ene oxidation, the weak ion signal at *m/z* = 126 indicates that the dominant pathway for R + O_2 reactions is through the HO_2-forming channel. Unlike in the other two isomers, only one conjugate alkene species is formed from 2,5-dimethylhex-3-ene, 2,5-dimethyl-1,4-hexadiene. Therefore, photoionization spectra are not required to identify the molecular structure of the specific C_8H_{14} isomer. The detection of time-resolved *m/z* = 110 on primary timescales confirms that 2,5-dimethylhex-3-ene, an intermediate oxidation product of 2,5-dimethylhexane oxidation, proceeds primarily through HO_2-forming pathways similar to Figure 1 in part by forming QOOH radicals that subsequently undergo unimolecular decomposition to form conjugate alkene.

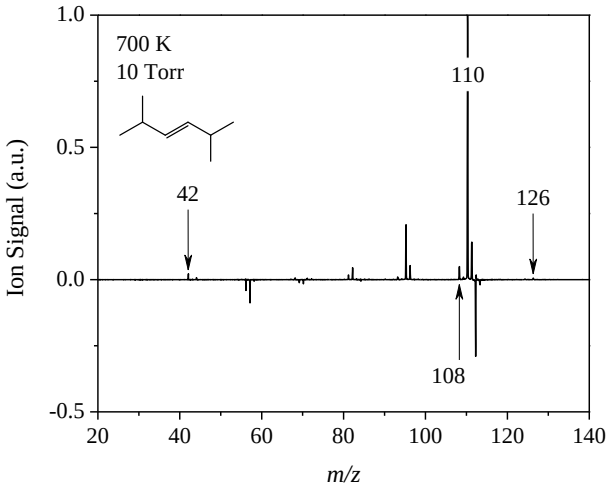

Figure 15. Difference mass spectrum of Cl-initiated oxidation of 2,5-dimethylhex-3-ene (*m/z* = 112); 700 K, 10 Torr. Negative ion signal indicates pre-photolysis photoionization of 2,5-dimethylhex-3-ene.

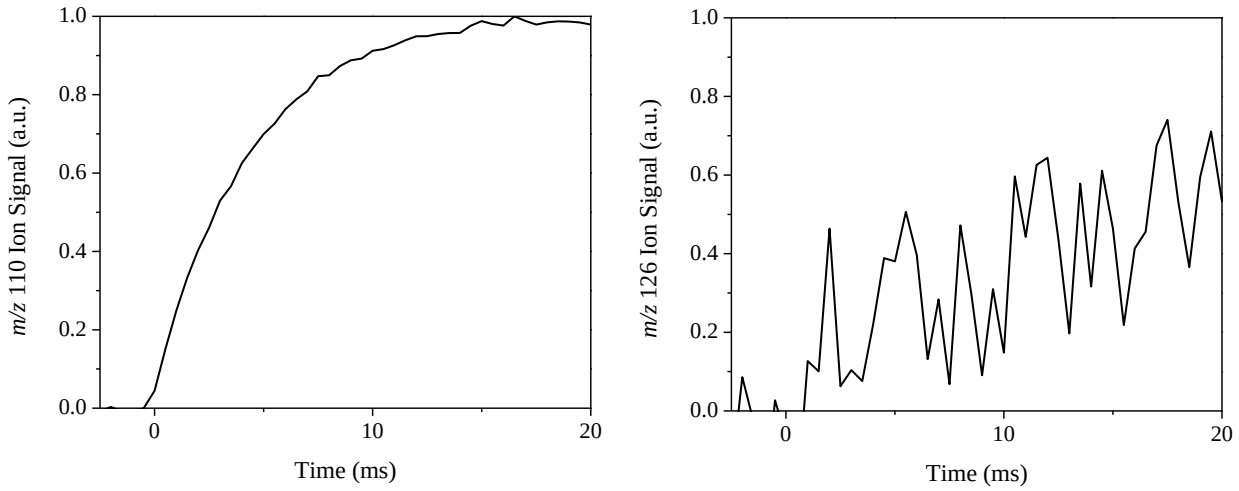

Figure 16. Time profiles of *m/z* = 110 (conjugate alkene) and *m/z* = 126 (cyclic ether / carbonyl) formed from oxidation of 2,5-dimethylhex-3-en-yl radicals.

In contrast to 2,5-dimethylhex-1- and -2-ene isomers, the symmetric molecular structure of 2,5-dimethylhex-3-ene results in a comparatively smaller number of chain-propagating and chain-terminating reactions on the R + O_2 potential energy surfaces of the two alkenyl radicals in Figure 14. The total number of reactions leading to *m/z* = 110 (i.e. 2,5-dimethyl-1,4-hexadiene), including both direct and sequential pathways, is 4, while the total number of QOOH-mediated reactions leading to *m/z* = 126 cyclic ether or carbonyl species coincident with OH is 8. Representative reactions leading to 2,5-dimethyl-1,4-hexadiene + HO_2 and *m/z* = 126 cyclic ether + OH are depicted in Figure 16.

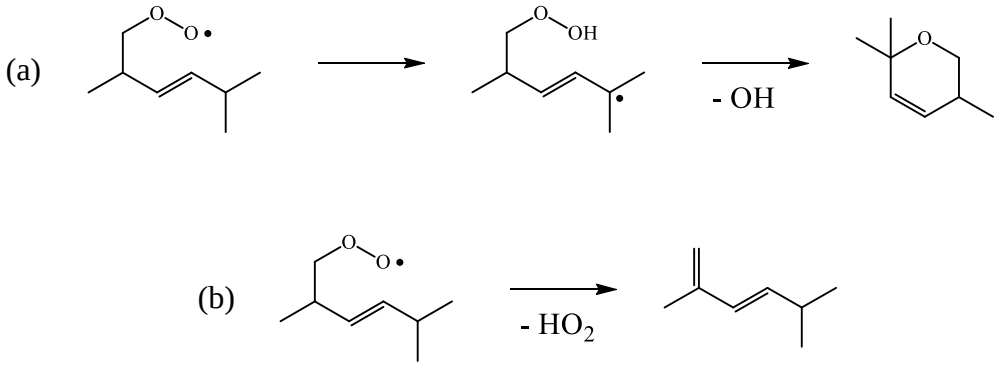

Figure 17. Initial R radicals formed in H-abstraction reactions of 2,5-dimethylhex-3-ene (vinylic radicals not depicted due to expected low yield from RH + Cl given the higher barrier to abstraction relative to alkylic sites [24, 25]).

R + O_2 chemistry, where R represents one of the two 2,5-dimethylhex-3-en-yl radical isomers in Figure 14 and that leads to the representative species in Figure 16, is not included for 2,5-dimethylhex-3-ene in the model of Sarathy et al. [14] model. Formation reactions in [14] leading to 2,5-dimethylhex-2-ene (Appendix, Table A3) include C–H β-scission of secondary 2,5-dimethylhex-3-yl radicals, direct formation via 2,5-dimethylhex-3-yl-peroxy radicals, and C–O bond-scission in β-QOOH radicals. The types of consumption reactions for 2,5-dimethylhex-2-ene in [14], written in the forward direction, are similar to reactions consuming 2,5-dimethylhex-1-ene and include: (1) abstraction reactions with OH/HO_2/H/CH_3/O yielding a single *lumped* species representing all 2,5-dimethylhex-*A*-en-*B*-yl radical isomers, (2) disproportionation reactions with OH/O, and (3) homolysis reactions yielding either yield alkenyl + alkyl or alkene + alkene. The (lumped) alkenyl radicals produced via H-abstraction from 2,5-dimethylhex-3-ene are only prescribed to undergo subsequent reaction with HO_2, methoxy (H_3CO), and ethoxy (H_3CCH_2O) and C–C β-scission reactions.

3.1.4. 2,2,5,5-tetramethyltetrahydrofuran

The two quaternary carbon atoms and molecular symmetry of 2,2,5,5-tetramethyltetrahydrofuran permits only two distinct initial radicals from H-abstraction reactions, a primary radical on one of the four methyl groups (Figure 19a) and a secondary radical on one of the two –CH_2– groups (Figure 19b). In addition, with only two distinct radicals and molecular symmetry the total number of reaction pathways on the two R + O_2 potential energy surfaces is comparatively smaller relative to the surfaces for initial radicals of either 2,5-dimethylhex-1-ene or 2,5-dimethylhex-2-ene. Well-depths similar to alkylperoxy radicals are expected for both types of radicals in Figure 18 given the absence of resonance stabilization in either structure. Cyclic ether or carbonyl species are associated with a nominal mass of parent *m/z* + 14 = *m/z* 142 and conjugate alkenes with a nominal mass of parent *m/z* – 2 = *m/z* = 126. The nominal mass-to-charge ratio of 2,2,5,5-tetramethyltetrahydrofuran is *m/z* = 128.

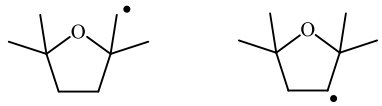

(a) (b)

Figure 18. Initial R radicals formed in H-abstraction reactions of 2,2,5,5-tetramethyltetrahydrofuran.

Figure 19 shows the background-subtracted photoionization mass spectrum of product species formed in Cl-initiated oxidation of 2,2,5,5-tetramethyltetrahydrofuran. The mass-to-charge ratios of primary oxidation products, formed directly from R + O_2 reactions, include *m/z* = 126 and *m/z* = 142, which correspond with conjugate alkene + HO_2 and cyclic ether/carbonyl + OH channels respectively. Compared to the mass spectra for the 2,5-dimethylhexene isomers (cf. Figure 7, Figure 11, Figure 15), the increase in the number of mass peaks in Figure 19 indicates an increased number of reactions involved in 2,2,5,5-tetramethyltetrahydrofuran; similar mass peaks include *m/z* = 42 (propene or ketene) and *m/z* = 68 (isoprene). The sources of other mass peaks remain unclear, e.g. *m/z* = 70, *m/z* = 82, *m/z* = 84, *m/z* = 108, and *m/z* = 112.

Time profiles were extracted from the background-subtracted mass spectra for *m/z* = 126 and *m/z* = 142 (Figure 20). The *m/z* = 126 time profile is composed of contributions from direct and sequential HO_2 formation mechanisms, the latter signifying the formation of QOOH radicals, yet because of ring-opening reactions the presence of other $C_8H_{14}O$ is possible. Similarly, the time-dependent signal at *m/z* = 142 also signifies the formation of QOOH radicals. Although absolute or relative photoionization spectra are required to identify the molecular structure of the specific $C_8H_{14}O$ and $C_8H_{14}O_2$ isomers, the detection of time-resolved *m/z* = 126 and *m/z* = 142 ion signals on primary timescales confirm that 2,2,5,5-tetramethyltetrahydrofuran, a cyclic ether intermediate of 2,5-dimethylhexane oxidation, proceeds through pathways similar to Figure 1 by forming QOOH radicals that subsequently undergo unimolecular decomposition to form conjugate alkene and cyclic ether or carbonyl species.

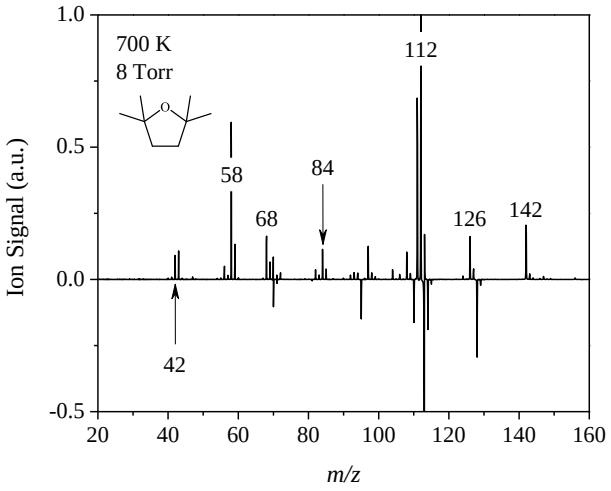

Figure 19. Difference mass spectrum of Cl-initiated oxidation of 2,2,5,5-tetramethyltetrahydrofuran (*m/z* = 128); 700 K, 10 Torr. Negative ion signal indicates pre-photolysis photoionization of 2,2,5,5-tetramethyltetrahydrofuran.

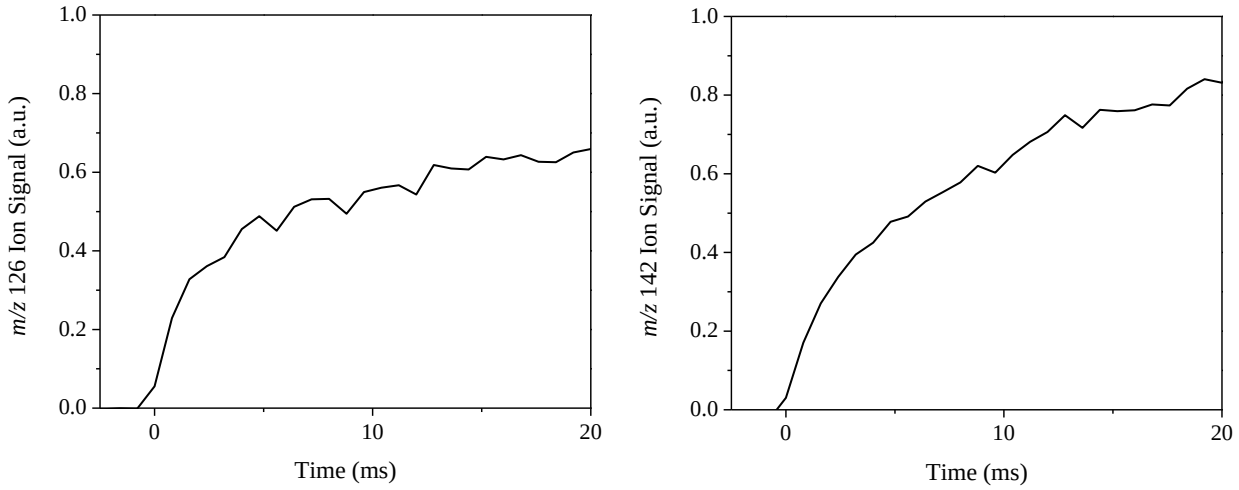

Figure 20. Time profiles of *m/z* = 126 (conjugate alkene) and *m/z* = 142 (cyclic ether / carbonyl) formed from oxidation of 2,2,5,5-tetramethyltetrahydrofuran-yl radicals.

The symmetry of 2,2,5,5-tetramethyltetrahydrofuran reduces the number of reactions on the R + O_2 potential energy surfaces of the two radicals depicted in Figure 18. Neglecting unimolecular decomposition via ring-opening, only two pathways leading to *m/z* = 126 exist, direct and sequential pathways to 2,2,5,5-tetramethyl-2,5-dihydrofuran + HO_2, and both are derived from the secondary radical. The number of QOOH-mediated reactions leading to *m/z* = 142 cyclic ether or carbonyl species coincident with OH is 6. Representative reactions leading to 2,2,5,5-tetramethyl-2,5-dihydrofuran and a bi-cyclic ether, 1,3,3-trimethyl-2,5-dioxabicyclo[2.2.1]heptane (*m/z* = 142), are depicted in Figure 21. Three other bi-cyclic ether species are possible, including and oxirane-type species derived from secondary R radicals (2,2,4,4-tetramethyl-3,6-dioxabicyclo[3.1.0]hexane), an oxetane-type species derived from either primary or secondary R radicals (1,3,3-trimethyl-2,6-dioxabicyclo[3.2.0]heptane), and an oxane-type species derived only from primary R radicals (1,5-dimethyl-3,8-dioxabicyclo[3.2.1]octane).

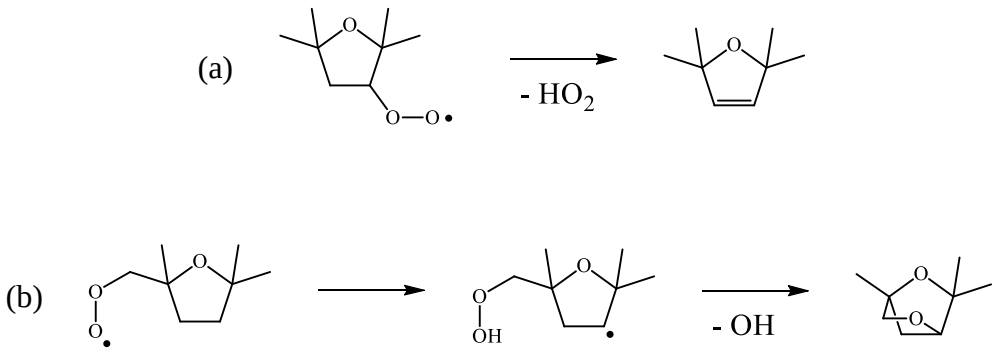

Figure 21. Representative reactions of peroxy radicals of 2,2,5,5-tetramethyltetrahydrofuran leading to (a) 2,2,5,5-tetramethyl-2,5-dihydrofuran (*m/z* = 126) and (b) 1,3,3-trimethyl-2,5-dioxabicyclo[2.2.1]heptane (*m/z* = 142).

Despite the importance of 2,2,5,5-tetramethyltetrahydrofuran in 2,5-dimethylhexane oxidation [16], and the comparatively small number of reactions on the two R + O_2 potential energy surfaces, only one type of consumption reaction is considered in the Sarathy et al. [14] model (Figure 22; Appendix, Table A5). The fate of 2,2,5,5-tetramethyltetrahydrofuran-yl radicals, whether by ring-opening neglected in favor of concerted decomposition via reaction with OH or HO_2 to form acetone + *iso*-penten-3-yl + H_2O/H_2O_2. Figure 23 depicts the bond-scission scheme leading to the products in Figure 22. Although the reactions in Figure 22 are plausible, the results from Figure 19 and Figure 20 indicate that some fraction of 2,2,5,5-tetramethyltetrahydrofuran remains intact and undergoes R + O_2 chemistry similar to that in Figure 1.

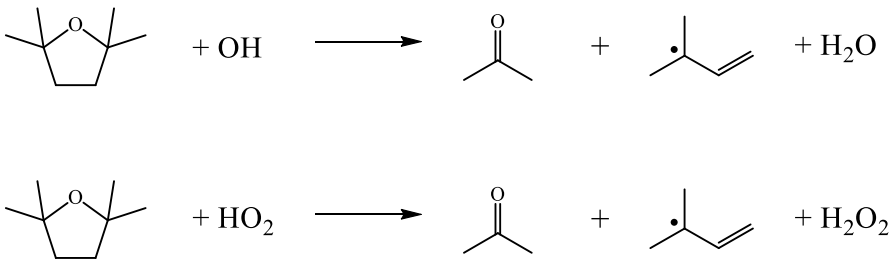

Figure 22. Reactions included in Sarathy et al. [14] for consumption of 2,2,5,5-tetramethyltetrahydrofuran.

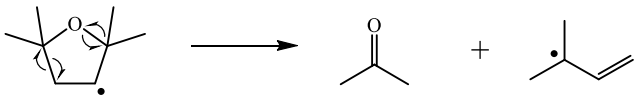

Figure 23. Bond-scission scheme for the sole decomposition mechanism included in Sarathy et al. [14] for 2,2,5,5-tetramethyltetrahydrofuran-yl radicals.

In addition to the abovementioned intermediates, several ring-opening reactions of initial R radicals introduce additional pathways that hold relevance to describing the low-temperature chemistry of 2,2,5,5-tetramethyltetrahydrofuran, particularly above 600 K where unimolecular decomposition competes with O_2-addition because of the ether group [17]. Figure 24 depicts one ring-opening reaction forming a tertiary radical, which can react with O_2 to form 2-methyl-2-(3-methylbut-3-en-1-yl)oxirane. Other ring-opening products include RO and a tertiary ether radical.

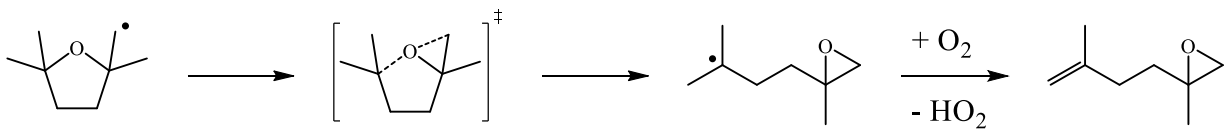

Figure 24. Reaction scheme for the formation of a *m/z* = 126 ($C_8H_{14}O$) isomer, 2-methyl-2-(3-methylbut-3-en-1-yl)oxirane, from reaction of O_2 with a ring-opened radical of 2,2,5,5-tetramethyltetrahydrofuran-1-yl with HO_2 as a co-product.

3.1.5. Summary on RO_2 chemistry of intermediates from 2,5-dimethylhexane oxidation

In comparing the mass spectra of the three alkene isomers, the effect of the C=C bond location is a diminished alkane-like oxidation chemistry due to the reduction in size of the aliphatic portion of the molecule as the C=C shifts from the terminal to the central position. The proximity of the C=C bond to the initial radical site influences reactivity in a similar manner to the results from methyl ester oxidation in Westbrook et al. [26]. The main cyclic ether intermediate formed in 2,5-dimethylhexane oxidation, 2,2,5,5-tetramethyltetrahydrofuran, exhibits complex low-temperature chemistry as indicated by the number of peaks in the mass spectrum. Although some portion of the mass peaks are attributable to photofragmentation, additional reactions from facile ring-opening of the initial R radicals is plausible.

Clear evidence of RO_2 chemistry is present in the Cl-initiated oxidation results of 2,5-dimethylhex-1-ene, 2,5-dimethylhex-2-ene, and 2,2,5,5-tetramethyltetrahydrofuran, evidenced in both the mass spectra and time profile measurements. No quantification of products is reported herein, as this requires absolute photoionization cross-sections of the different isomers that comprise the mass channels. However, of particular significance is the comparable ion signal intensities for nominal *m/z* that are directly reflective of cyclic ether (or carbonyl) species being formed from R + O_2 indicating that QOOH formation is appreciable in such cases. The third alkene isomer, 2,5-dimethylhex-3-ene, also exhibits RO_2 chemistry yet mainly in the form of HO_2 + 2,5-dimethylhexa-1,3-diene. Only marginal cyclic ether signal is detected, indicating negligible QOOH formation is occurring. However, in addition to QOOH formation being the central focus in the present context, in cases where the concentrations of primary oxidation intermediates are appreciable, the impact at a minimum is on the mechanistic budgeting for the consumption of certain radicals, namely OH and HO_2, which are most relevant at temperatures below ca. 1000 K.

The comprehensive chemical kinetics model of Sarathy et al. [14] contains 883 species and 4204 reactions. In present form, the model of [14] approaches the oxidation of the 2,5-dimethylhexene isomers by employing a commonly invoked lumping procedure for alkenyl radicals from all three isomers in which a single radical – 2,5-dimethylhex-A-en-B-yl. Consumption reactions of 2,5-dimethylhex-A-en-B-yl do not include reaction with O_2, only disproportionation reactions involving H-abstraction by HO_2, methylperoxy (H_3COO), and ethylperoxy ($H_3CCH_2O_2$), forming (ac3h5cho) + *iso*-butenyl + OH/methoxy/ethoxy, and C–C β-scission to yield alkyl + alkene (Appendix, Table A4). Similarly, only two reactions are prescribed to account for the fate of 2,2,5,5-tetramethyltetrahydrofuran. If the various isomers behave sufficiently different in subsequent oxidation steps, the neglect of such channels in the development of comprehensive chemical kinetics models may adversely impact the mechanistic description of peroxy radical chemistry that drives autoignition, even in cases such as 2,5-dimethylhex-3-ene where QOOH formation is less significant. Given the abundance [14] of the four primary oxidation intermediates studied, which are demonstrated here to exhibit low-temperature R + O_2 chemistry, including sub-mechanisms that take into account isomer-specific R + O_2 reactions may lead to a more-complete and more-robust chemical description of autoignition and other combustion processes modeled using comprehensive chemical kinetics mechanisms.

3.2. Product Formation from R + O_2 Reactions of Intermediates Formed in Cyclohexane Oxidation

Experimental and computational studies on cyclohexane oxidation at temperatures below 1000 K include: jet-stirred reactor (JSR) measurements coupled with comprehensive chemical kinetics modeling (El Bakali et al. [27], Silke et al. [13], and Serinyel et al. [15]), measurements of OH and HO_2 time profiles and *ab initio* calculations of cyclohexyl + O_2 reactions (Fernandes et al. [28] and Knepp et al. [29], respectively), and MPIMS measurements of cyclohexene branching fractions (Rotavera et al. [17]). In the latter two JSR studies, cyclohexene oxide (referred to as 1,2-epxoycyclohexane) is underpredicted in both models, by up to a factor of five at dilute conditions [15] and non-dilute conditions [13]. Because of the inaccuracies in predicting concentrations of cyclohexene oxide, and other species, Silke et al. [13] remarked on the potential for deficiency in relying on conventional R + O_2 modeling approaches following the paradigm outlined in Figure 1. In all three JSR studies, cyclohexene is a major intermediate from cyclohexane oxidation yet is either over- or underpredicted below 1000 K. Rotavera et al. [17] conducted MPIMS measurements at conditions similar to the present experiments (10 Torr and 500 K – 700 K), and at 700 K reported that the branching fraction to cyclohexene + HO_2 from R + O_2 approached 35% and 10 Torr and 20% at 1500 Torr. Given the positive temperature dependence associated with R + O_2 → conjugate alkene + HO_2 in alkane oxidation, cyclohexene is expected to be of considerable importance above ca. 700 K

Similar to other olefinic molecules, e.g. 2,5-dimethylhexene isomers, product formation from reaction of cyclohexenyl isomers with O_2 follows, in part, the oxidation paradigm in Fig. 1 with additional reactions likely involved, including radical-addition to unsaturated carbon, retroene reactions, and others. Alkene-specific reactions augmenting Fig. 1 that account for unsaturated carbon are discussed in studies on hexene isomers, e.g. Mehl et al. [9], Bounaceur et al. [10], and Battin-Leclerc et al. [11]. Reactions of O_2 with either of the two types of radicals of cyclohexene oxide are expected to exhibit similarity with the alkane sequence in Fig. 1, due to the absence of sp^2 carbon, although the presence of an ether group promotes ring-opening reactions in initial R radicals, which competes with O_2-addition and subsequent ROO or QOOH formation [17].

3.2.1. Cyclohexene

Initiation reactions via H-abstraction in cyclohexene oxidation lead to three distinct initial radicals, all of which are secondary, distinguished as either alkylic (Figure 25a), allylic (Figure 25b), or vinylic. The latter type of radical is not considered herein due to higher barriers to abstraction relative to alkylic sites [24, 25] resulting in negligible branching fractions, particularly at temperatures below 800 K. Resonance-stabilized radicals are formed in abstraction reactions involving allylic H atoms, which results in similar effects on well-depths for peroxy adducts as discussed in Section 3.1, i.e. O_2-addition to alkylic sites being ~35 kcal/mol exothermic and O_2-addition to resonance-stabilized radicals approximately 20 kcal/mol exothermic. In both cases, however, the formation of both cyclic ether and carbonyl species (i.e. parent m/z + 14) and conjugate alkenes (i.e. parent m/z – 2) is expected. The nominal mass-to-charge ratio of cyclohexene is m/z = 82.

Figure 25. Initial R radicals formed in H-abstraction reactions of cyclohexene (vinylic radicals not depicted due to higher barrier to abstraction relative to alkylic sites [24, 25]).

Figure 26 shows the background-subtracted photoionization mass spectrum of product species formed in Cl-initiated oxidation of cyclohexene. The mass-to-charge ratios of primary oxidation products, formed directly from R + O_2 reactions, include *m/z* = 80 and *m/z* = 96, which correspond with conjugate alkene + HO_2 and cyclic ether/carbonyl + OH channels respectively. *m/z* = 78 is consistent with the formation of benzene (C_6H_6), which is arises from reaction of O_2 with allylic cyclohex-1-en-3-yl or alkylic cyclohex-1-en-4-yl radicals. The identity of other mass peaks is unclear. However, since ring-opening reactions are not significant under the experimental conditions used in Figure 26 [17] the other mass peaks may result from photofragmentation.

Time profiles were extracted from the background-subtracted mass spectra for *m/z* = 80 and *m/z* = 96 (Figure 27). The *m/z* = 80 time profile is composed of contributions from direct and sequential HO_2 formation mechanisms, the latter signifying the formation of QOOH radicals, and is likely to consist primarily of 1,3-cyclohexadiene and 1,4-cyclohexadiene with marginal contribution from 1,2-cyclohexadiene due to the required abstraction of vinylic hydrogen. Similarly, and perhaps more directly, the time-dependent signal at *m/z* = 96 also signifies the formation of QOOH radicals. Although the absolute or relative photoionization spectra are required to identify the molecular structure of the specific C_6H_{10} and $C_6H_{10}O$ isomers, the detection of time-resolved *m/z* = 80 and *m/z* = 96 ion signals on primary timescales confirm that cyclohexene, a significant intermediate of cyclohexane oxidation, proceeds through pathways similar to Figure 1 by forming QOOH radicals that subsequently undergo unimolecular decomposition to form conjugate alkene and cyclic ether/carbonyl species.

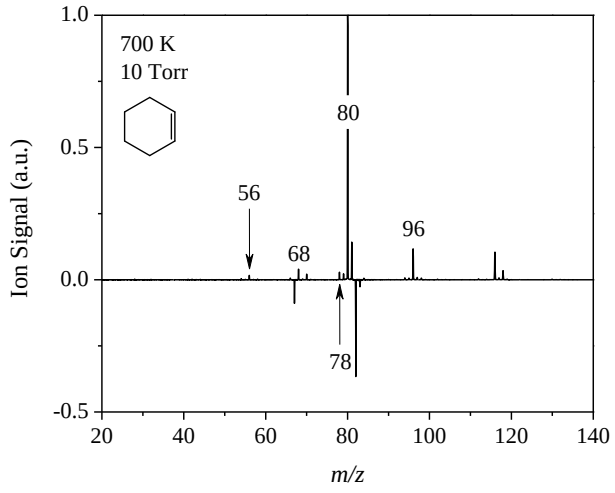

Figure 26. Difference mass spectrum of Cl-initiated oxidation of cyclohexene (*m/z* = 82); 700 K, 10 Torr. Negative ion signal indicates pre-photolysis photoionization of cyclohexene.

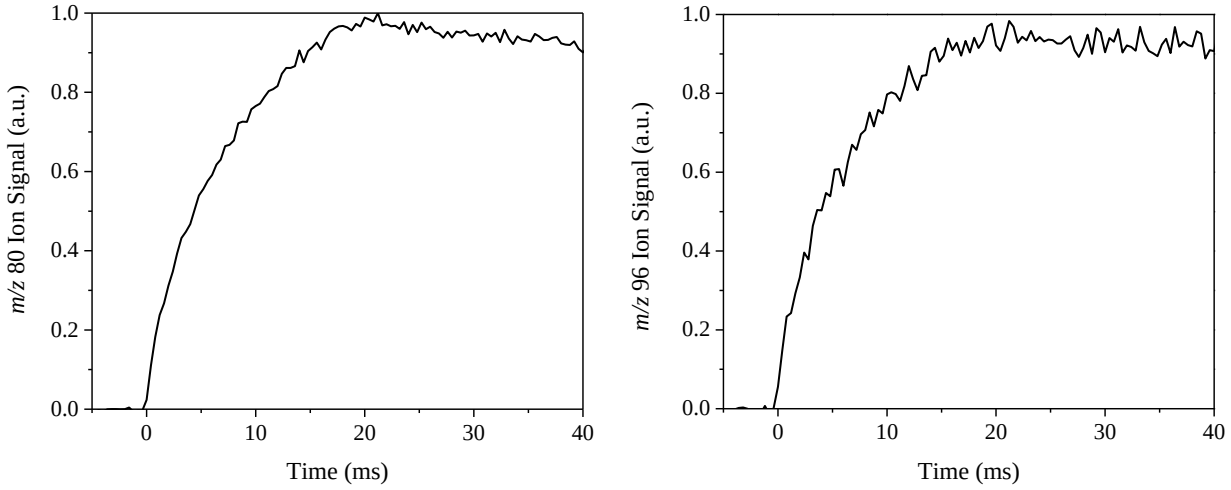

Figure 27. Time profiles of *m/z* = 80 (conjugate alkene) and *m/z* = 96 (cyclic ether / carbonyl) formed from oxidation of cyclohexenyl radicals.

The symmetry of cyclohexene reduces the number of reactions on the R + O_2 potential energy surfaces of the two radicals depicted in Figure 25. Neglecting contributions from vinylic radicals and unimolecular decomposition via ring-opening of the alkylic and allylic radicals, four pathways leading to *m/z* = 80 exist on both surfaces. For the alkylic cyclohex-1-en-4-yl + O_2 surface, direct and sequential pathways to 1,3- and 1,4-cyclohexadiene, and for the allylic cyclohex-1-en-3-yl + O_2 surface, direct and sequential pathways to 1,2- and 1,3-cyclohexadiene. The number of QOOH-mediated reactions leading to *m/z* = 96 cyclic ether / carbonyl + OH is 8 (neglecting ring-opening reactions and vinylic H-abstraction). Representative reactions leading to 1,3-cyclohexadiene and a bi-cyclic ether, 7-oxabicyclo[4.1.0]hept-2-ene (*m/z* = 96), are depicted in Figure 28.

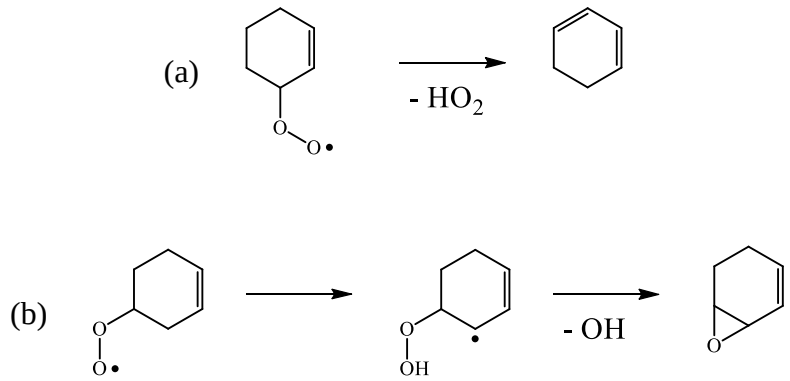

Figure 28. Representative reactions of peroxy radicals of cyclohexene leading to (a) 1,3-cyclohexadiene (*m/z* = 80) and (b) 7-oxabicyclo[4.1.0]hept-2-ene (*m/z* = 96).

R + O_2 chemistry, where R represents one of the two cyclohexenyl radical isomers in Figure 25, that leads to the representative species in Figure 28 is not included for cyclohexene in the abovementioned models [13, 15, 27] despite the importance to cyclohexane oxidation. Only several reactions are included in the comprehensive chemical kinetics mechanisms of Silke et al.

[13] and Serinyel et al. [15], while the El Bakali et al. [27] model does not include peroxy radical chemistry. Consumption reactions for cyclohexene in Silke et al. [13] (Appendix, Table A12) include several H-abstraction reactions initiated by H/CH_3/O/OH/HO_2 to form either alkylic cyclohex-1-en-4-yl or allylic cyclohex-1-en-3-yl, unimolecular decomposition into ethene + C_4H_6 (butyne isomer), and radical-addition reactions involving HO_2 and H. Silke et al. [13] define radical-specific chemistry to the alkylic and allylic cyclohexyl radicals, rather than invoking a lumping procedure. Four reactions in total are included for consumption of alkylic cyclohex-1-en-4-yl (Appendix, Table A13) in [13]. Separate from the two reverse reactions describing the formation of cyclohex-1-en-4-yl, two additional reactions are written: C–H β-scission into 1,3-cyclohexadiene + H and isomerization via ring-opening into 1,5-hexadien-5-yl (hx14en6j). The same four reactions are applied to allylic cyclohex-1-en-3-yl (Appendix, Table A14), however two additional reactions are included: reaction with O_2 to form 1,3-cyclohexadiene + HO_2 and reaction with HO_2 to form an oxygen-centered radical + OH.

Serinyel et al. [15] adopts a similar approach using isomer-specific reaction sets. Consumption of alkylic cyclohex-1-en-4-yl is described by the reactions below, the rate parameters for which are listed in the Appendix, Table A7.

1. disproportionation with HO_2 to form OH + formyl + cyclopentene (C5H8#5)
2. reaction with O_2 to form alkenyl + HO_2
3. reaction with HO_2 to form OH + $H_2CC(=O)H$ (H2CCHO) + butadiene (C4H6Z2)
4. isomerization to give cyclohex-1-en-3-yl
5. isomerization to a linear radical (RC6H9ZX)

Similarly, consumption of allylic cyclohex-1-en-3-yl is described by the reactions below and the rate parameters are listed in the Appendix, Table A8.

1. reaction with HO_2 to give OH + formyl + cyclopentene (C5H8#5)
2. reaction with O_2 to give HO_2 + 1,3-cyclohexadiene (C6H8#6-13)
3. reaction with HO_2 to give OH + ethene + CO + allyl (R104C3H5Y)
4. isomerization to cyclohex-1-en-4-yl (RC1C6H9#6Z) and vinylic cyclohex-1-en-2-yl (RC3C6H9#6V)
5. isomerization to a linear radical (RC6H9ZY)

3.2.2. Cyclohexene oxide

Three distinct initial radicals form from H-abstraction reactions of cyclohexene oxide, two secondary radicals (Figure 29a and 29b) and a tertiary radical adjacent to the epoxy group (Figure 29c). RO_2 well-depths similar to alkylperoxy radicals are expected for all three radicals in Figure 29 given the absence of resonance stabilization in the molecular structures. Cyclic ether or carbonyl species are associated with a nominal mass of parent $m/z + 14 = m/z = 126$ and conjugate alkenes with a nominal mass of parent $m/z - 2 = m/z = 96$. The nominal mass-to-charge ratio of cyclohexene oxide is $m/z = 98$.

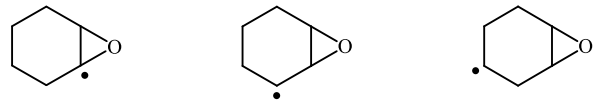

(a) (b) (c)

Figure 29. Initial R radicals formed in H-abstraction reactions of cyclohexene oxide.

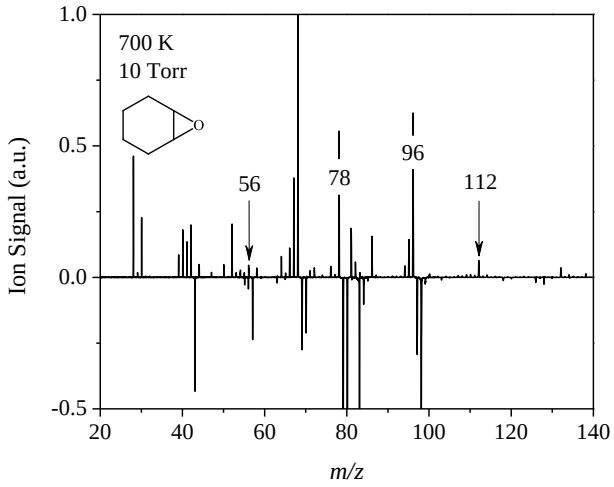

Figure 30. Difference mass spectrum of Cl-initiated oxidation of cyclohexene oxide (*m/z* = 98); 700 K, 10 Torr. Negative ion signal indicates pre-photolysis photoionization of cyclohexene oxide.

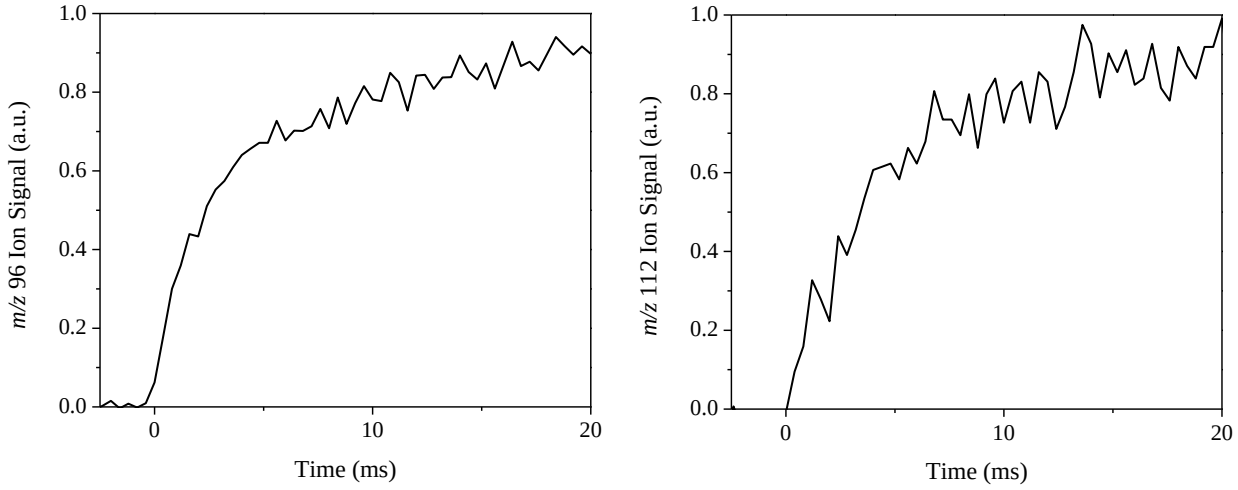

Figure 31. Time profiles of *m/z* = 96 (conjugate alkene) and *m/z* = 112 (cyclic ether / carbonyl) formed from oxidation of radicals of cyclohexene oxide.

The R + O_2 potential energy surfaces of the three radicals depicted in Figure 29 comprise a significant number of reaction pathways. For the R + O_2 surface of the tertiary radical in Figure 30a, two direct and two sequential pathways exist, leading to one of two different isomers: 7-oxabicyclo[4.1.0]hept-1(6)-ene or 7-oxabicyclo[4.1.0]hept-1-ene. Similarly, for the R + O_2 surface

of the secondary radical in Figure 29b, two direct and two sequential pathways exist, leading to two different isomers: 7-oxabicyclo[4.1.0]hept-1-ene or 7-oxabicyclo[4.1.0]hept-2-ene, and for the surface of the secondary radical in Figure 30c, two direct and two sequential pathways exist, leading to two different isomers: 7-oxabicyclo[4.1.0]hept-2-ene or 7-oxabicyclo[4.1.0]hept-3-ene. The total number of QOOH-mediated reactions leading to *m/z* = 96 cyclic ether / carbonyl + OH is 16. Representative reactions leading to 1,3-cyclohexadiene and a bi-cyclic ether, 7-oxabicyclo[4.1.0]hept-2-ene (*m/z* = 96), are depicted in Figure 32.

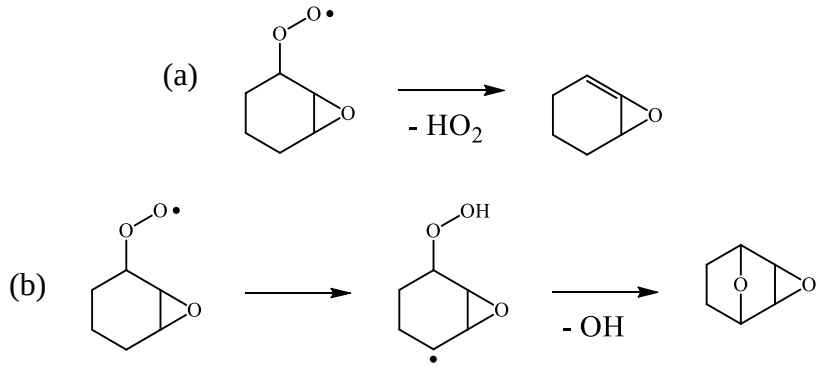

Figure 32. Representative reactions of peroxy radicals of cyclohexene oxide leading to (a) 7-oxabicyclo[4.1.0]hept-1-ene (*m/z* = 80) and (b) 3,8-dioxatricyclo[3.2.1.$0^{2,4}$]octane (*m/z* = 96).

Consumption reactions of cyclohexene oxide in Silke et al. [13] (Appendix, Table A15) include H-abstraction by OH/H/CH_3/HO_2 forming a lumped radical for cyclohexene oxide (chx1*o2j) and an addition reaction involving formyl (HCO) leading to a $C_7H_{11}O_2$ radical (chxcho2oj). The lumped radical chx1*o2j is prescribed to undergo reactions accounting only for ring-opening via homolysis, into either vinyl + CH_2CO + ethene or ethene + ethene + HCCO. Isomerization of chx1*o2j via ring-opening to a linear radical is also included. However, no reactions of the lumped radical with O_2 are included (Appendix, Table A16). Serinyel et al. [15] adopts a similar approach, yet excludes addition reactions to cyclohexene oxide (Appendix, Table A10). H-abstraction reactions with H/OH/HO_2/CH_3/CH_3OO/C_2H_5 form a lumped cyclic ether radical of the molecular formula C_6H_9O (RC6H9#6OK). The lumped radical is then prescribed to react via one of two pathways (Appendix, Table A11): isomerization via ring-opening into a linear radical (RC6H9OZ) or reaction with O_2 to form a generic olefinic cyclic ether (C6H8O#6KZ) + HO_2 in a chain-inhibiting step.

3.2.3. Summary on RO_2 chemistry of intermediates from cyclohexane oxidation

Clear evidence of RO_2 chemistry is present in the Cl-initiated oxidation results of both cyclohexene and cyclohexene oxide (1,2-epoxycyclohexane), evidenced in both the mass spectra and time profile measurements. Although no quantification of products is reported herein, which requires absolute photoionization cross-sections of the different isomers that comprise the mass channels, of particular significance is the comparable ion signal intensities for nominal *m/z* that are directly

reflective of cyclic ether (or carbonyl) species being formed from R + O_2 indicating that QOOH formation is appreciable in such cases. The mass spectrum results from cyclohexene oxidation, in which only two main product peaks appeared, *m/z* = 80 and *m/z* = 96, indicate that ring-opening of cyclohexenyl radicals is unlikely to be significant at temperatures ≤ 700 K. Detection of both the conjugate alkene (*m/z* = 80) and cyclic ether/carbonyl (*m/z* = 96) time profiles, which occurred on identical timescales, indicate that QOOH formation is relevant to cyclohexene oxidation.

In contrast, the mass spectrum results from Cl-initiated oxidation of cyclohexene oxide, revealed numerous product peaks formed separate from the two main RO_2-mediated products peaks, *m/z* = 96 and *m/z* = 112. The time profiles of both *m/z* = 96 and *m/z* = 112 are on primary timescales (stemming from R + O_2), indicating the relevance of both mass peaks and also providing evidence on the formation of preceding QOOH radicals. Photofragmentation is likely responsible for certain mass peaks, however given the tendency of oxygen-containing rings to undergo ring-opening [17], the formation of linear radicals which undergo subsequent oxidation reactions leading to some of the product peaks in Figure 30 is also plausible. Unimolecular decomposition of the tertiary radical (Figure 30c) is likely facile considering the proximity of the unpaired electron to the oxygen heteroatom. In addition to unimolecular decomposition via ring-opening, a rearrangement reaction is plausible wherein the tertiary radical converts into the resonance-stabilized radical 2-oxocyclohexyl (α radical of cyclopentanone), Figure 33, which can subsequently react with O_2 to form QOOH radicals.

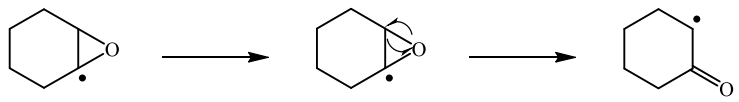

Figure 33. Rearrangement reaction of the tertiary radical of cyclohexene oxide forming 2-oxocyclohexyl.

Only a limited number of studies exist on cyclohexene oxidation [30-32]. The shock-tube ignition delay time measurements Dayma et al. [30] were conducted at temperatures above 1000 K therefore the chemical kinetics model developed did not include peroxy radical chemistry. Lemaire et al. [31] used RCM-speciation experiments to postulate reaction mechanisms leading to benzene from cyclohexene at temperature between 600 K and 900 K, relying on yield measurements of conjugate alkenes, bicyclic ethers, and linear/cyclic carbonyl species. Ribaucour et al. [32] developed the only existing low-temperature cyclohexene model, which is composed of 136 species and 1064 reactions and accounts for prototypical R + O_2 chemistry including, for example, cyclic ether formation, and radical-addition reactions (e.g. OH + cyclohexene = cyclohexan-1-ol-2-yl). The reaction scheme outlining the majority of the types of reactions included in the model is presented in [32], yet it is unclear if reactions of the primary oxidation intermediates is included.

For the results above, at conditions where the concentrations of primary oxidation intermediates (e.g. cyclohexene and cyclohexene oxide) are comparable with the parent molecule (e.g. cyclohexane), these products compete with the initial fuel for reaction with OH, HO_2, and other abstracting radicals. These H-abstractions produce hydrocarbon radicals that will in turn react with O_2, so the role of R + O_2 chemistry of primary oxidation intermediates in accurately modeling the oxidation and autoignition of cyclohexane can be expected to become prominent.

Both cyclohexene and cyclohexene oxide were detected in similar concentrations in both RCM-speciation measurements [13] and JSR-speciation measurements [15]. Other cyclic ether species (e.g. 1,4-epoxycyclohexane) and the ring-opened aldehyde 5-hexenal, which are also produced in appreciable concentrations, are important to consider and likely to undergo R + O_2 chemistry, as with cyclohexene, and form QOOH radicals. Neither species are prescribed peroxy radical chemistry in the existing cyclohexane models [13, 15]. In addition to QOOH formation being the central focus in the present context, in cases where the concentrations of primary oxidation intermediates are appreciable, the impact at a minimum is on the mechanistic budgeting for the consumption of certain radicals, namely OH and HO_2, which are most relevant at temperatures below ca. 1000 K.

3.3. Product Formation from R + O_2 Reactions of Intermediates Formed in Tetrahydropyran Oxidation

Oxidation studies of tetrahydropyran include speciation measurements in JSR and plug flow reactor experiments [33, 34] and in laminar flame molecular beam mass spectrometry experiments [35], all of which were conducted under conditions where peroxy radical chemistry is unimportant. Consequently, the two comprehensive chemical kinetics mechanisms present in the literature [33, 34] exclude peroxy radical chemistry. The sole low-temperature study of tetrahydropyran is the MPIMS study of Rotavera et al. [17], wherein Cl-initiated oxidation experiments were conducted to directly measure conjugate alkene branching fractions from reactions of tetrahydropyranyl radicals with O_2. The two conjugate alkene isomer intermediates from R + O_2 reactions of tetrahydropyran, 3,4- and 3,6-dihydro-*2H*-pyran, were quantified in [17] and at 700 K accounted for a combined 20% of the branching fraction of R radicals, at 10 Torr, and 10% at 1500 Torr; negative temperature dependence was reported for oxygen concentrations on the order of 10^{16} molecules cm^{-3} due to ring-opening of initial R radicals outcompeting O_2 addition [17].

3,4- and 3,6-dihydro-*2H*-pyran combine unique molecular motifs in that both contain oxygen heteroatoms, giving rise to the importance of ring-opening of initial R radicals, and sp^2 carbon which permits radical-addition reactions and the formation of resonance-stabilized R and QOOH radicals. Correspondingly, the development of a low-temperature reaction mechanism for tetrahydropyran that accounts for R + O_2 reactions of primary oxidation intermediates must include alkene-specific reactions similar to those discussed in studies on hexene isomers, e.g. Mehl et al. [9], Bounaceur et al. [10], and Battin-Leclerc et al. [11], and must include ring-opening reactions of initial R (both for tetrahydropyran and the related primary oxidation intermediates).

3.3.1. 3,4-dihydro-2H-pyran

Neglecting abstraction of vinylic hydrogen, three distinct initial radicals form from H-abstraction reactions of 3,4-dihydro-*2H*-pyran; one allylic radical (Figure 34a), one alkylic radical (Figure 34b), and one α radical adjacent to the –O– group (Figure 34c). With the exception of O_2-addition to the α site forming RO_2 in the equatorial position, which is slightly higher in energy relative to addition to the axial position by approximately 4 kcal/mol [17], an RO_2 well-depth similar to alkylperoxy radicals is expected for the radical in Figure 34b, while for the allylic radical in Figure 34c a well-depth for RO_2 of approximately 20 kcal/mol is expected. Cyclic ether or carbonyl species are associated with a nominal mass of parent *m/z* + 14 = *m/z* = 98 and conjugate alkenes with a nominal mass of parent *m/z* – 2 → 82. The nominal *m/z* of 3,4-dihydro-*2H*-pyran is 84.

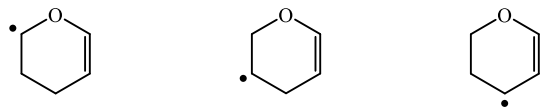

(a) (b) (c)

Figure 34. Initial R radicals formed in H-abstraction reactions of 3,4-dihydro-*2H*-pyran (vinylic radicals are not depicted due to higher barrier to abstraction relative to alkylic sites [24, 25]).

Figure 35 shows the background-subtracted photoionization mass spectrum of product species formed in Cl-initiated oxidation of 3,4-dihydro-*2H*-pyran. The mass-to-charge ratios of primary oxidation products, formed directly from R + O_2 reactions, include *m/z* = 82 and *m/z* = 98, which correspond with conjugate alkene + HO_2 and cyclic ether/carbonyl + OH channels respectively. The absence of *m/z* = 80 indicates that no further reaction proceeds after the conjugate alkene isomers are formed as no available H is present. The identity of the other mass peaks is unclear. However, since ring-opening reactions are significant under the experimental conditions used in Figure 35 [17], the other mass peaks may result from oxidation reactions of ring-opened radicals in addition to photofragmentation.

Time profiles were extracted from the background-subtracted mass spectra for *m/z* = 82 and *m/z* = 98 (Figure 36). The *m/z* = 82 time profile is composed of contributions from direct and sequential HO_2 formation mechanisms, the latter signifying the formation of QOOH radicals, and consists of *2H*-pyran and/or *4H*-pyran due to the required abstraction of vinylic hydrogen for the formation of the remaining *m/z* = 82 isomer. Similarly, and perhaps more directly, the time-dependent signal at *m/z* = 98 also signifies the formation of QOOH radicals. Although the absolute or relative photoionization spectra are required to identify the molecular structure of the specific C_5H_6O and $C_5H_6O_2$ isomers, the detection of time-resolved *m/z* = 82 and *m/z* = 98 ion signals on primary timescales confirm that 3,4-dihydro-*2H*-pyran, an intermediate of tetrahydropyran oxidation, proceeds through pathways similar to Figure 1 by forming QOOH radicals that subsequently undergo unimolecular decomposition to form conjugate alkene and cyclic ether / carbonyl species.

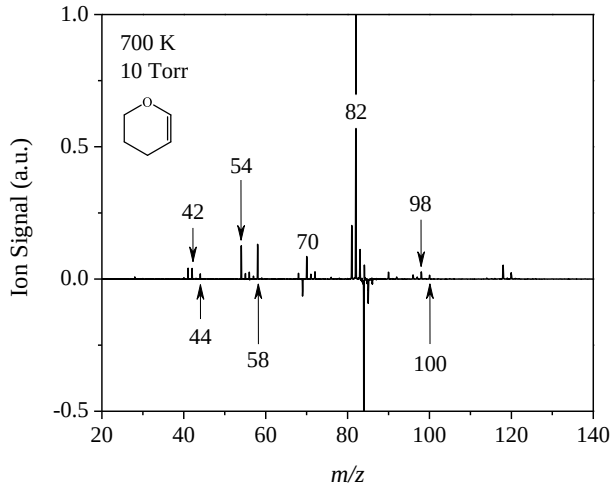

Figure 35. Difference mass spectrum of Cl-initiated oxidation of 3,4-dihydro-*2H*-pyran (*m/z* = 84); 700 K, 10 Torr. Negative ion signal indicates pre-photolysis photoionization of 3,4-dihydro-*2H*-pyran.

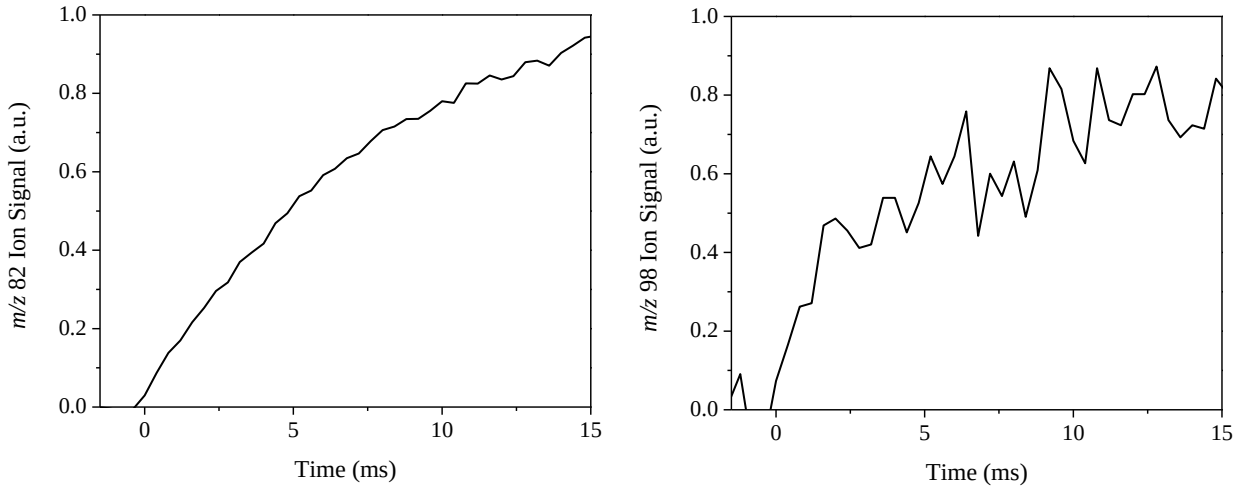

Figure 36. Time profiles of *m/z* = 82 (conjugate alkene) and *m/z* = 98 (cyclic ether / carbonyl) formed from oxidation of 3,4-dihydro-*2H*-pyranyl radicals.

The asymmetry of 3,4-dihydro-*2H*-pyran adds complexity to the R + O_2 potential energy surfaces of the three radicals depicted in Figure 34. However, neglecting reaction pathways involving vinylic hydrogen, only oxirane- and oxetane-type cyclic ether pathways exist on all three surfaces, in addition to a ketone-forming pathways. Accounting for both direct and sequential HO_2-forming mechanisms, two pathways exist on the surface of the α radical, forming *4H*-pyran, four pathways on the surface of the alkylic radical, forming both *2H*- and *4H*-pyran, and two pathways on the surface of the allylic radical, forming only *2H*-pyran. The total number of QOOH-mediated reactions leading to *m/z* = 98 cyclic ether or carbonyl species coincident with OH on the three surfaces is 9 (neglecting ring-opening reactions and vinylic H-abstraction). Representative reactions leading to *4H*-pyran (*m/z* = 82) and a bi-cyclic ether, 2,7-dioxabicyclo[4.1.0]hept-3-ene (*m/z* = 98), are depicted in Figure 37.

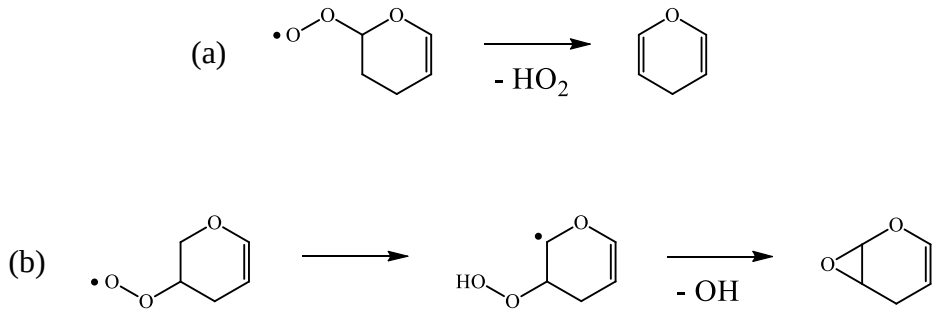

Figure 37. Representative reactions of peroxy radicals of 3,4-dihydro-*2H*-pyran leading to (a) 4*H*-pyran (*m/z* = 82) and (b) 2,7-dioxabicyclo[4.1.0]hept-3-ene (*m/z* = 98).

3.3.2. 3,6-dihydro-2H-pyran

Neglecting abstraction of vinylic hydrogen, three distinct initial radicals form from H-abstraction reactions of 3,4-dihydro-*2H*-pyran; one α radical adjacent to the –O– group (Figure 38a) and two allylic radicals (Figure 38b and 38c). With the exception of O_2-addition to the α site forming RO_2 in the equatorial position, which is slightly higher in energy by approximately 4 kcal/mol [17], an RO_2 well-depth similar to peroxy radicals formed from O_2-addition to resonance-stabilized R radicals is expected for the radicals in Figures 38b and 38c. Cyclic ether or carbonyl species are associated with a nominal mass of parent $m/z + 14 = m/z = 98$ and conjugate alkenes with a nominal mass of parent $m/z - 2 = m/z = 82$. The nominal mass-to-charge ratio of 3,6-dihydro-*2H*-pyran is $m/z = 84$.

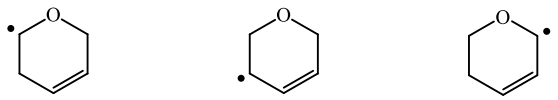

(a) (b) (c)

Figure 38. Initial R radicals formed in H-abstraction reactions of 3,6-dihydro-*2H*-pyran (vinylic radicals not depicted due to higher barrier to abstraction relative to alkylic sites [24, 25]).

Figure 39 shows the background-subtracted photoionization mass spectrum of product species formed in Cl-initiated oxidation of 3,6-dihydro-*2H*-pyran. The mass-to-charge ratios of primary oxidation products, formed directly from R + O_2 reactions, include $m/z = 82$ and $m/z = 98$, which correspond with conjugate alkene + HO_2 and cyclic ether/carbonyl + OH channels respectively. The absence of $m/z = 80$ indicates that no further reaction proceeds after the conjugate alkene isomers are formed as no available H is present. The identity of the other mass peaks is unclear. However, since ring-opening reactions are significant under the experimental conditions used in Figure 39 [17], the other mass peaks may result from oxidation reactions of ring-opened radicals in addition to photofragmentation.

Time profiles were extracted from the background-subtracted mass spectra for $m/z = 82$ and $m/z = 98$ (Figure 40). The $m/z = 82$ time profile is composed of contributions from direct and sequential HO_2 formation mechanisms, the latter signifying the formation of QOOH radicals, and consists only of *2H*-pyran due to the required abstraction of vinylic hydrogen for the formation of the remaining $m/z = 82$ isomers. Similarly, and perhaps more directly, the time-dependent signal at $m/z = 98$ also signifies the formation of QOOH radicals. Although the absolute or relative photoionization spectra are required to identify the molecular structure of the specific C_5H_6O and $C_5H_6O_2$ isomers, the detection of time-resolved $m/z = 82$ and $m/z = 98$ ion signals on primary timescales confirm that 3,6-dihydro-*2H*-pyran, an intermediate of tetrahydropyran oxidation, proceeds through pathways similar to Figure 1 by forming QOOH radicals that subsequently undergo unimolecular decomposition to form conjugate alkene and cyclic ether/carbonyl species.

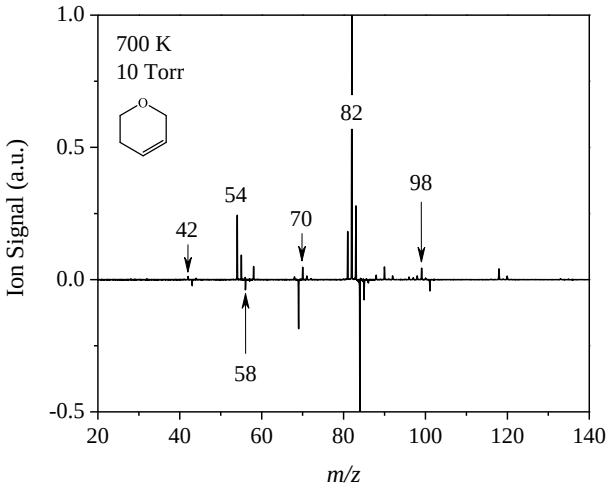

Figure 39. Difference mass spectrum of Cl-initiated oxidation of 3,6-dihyro-*2H*-pyran (*m/z* = 84); 700 K, 10 Torr. Negative ion signal indicates pre-photolysis photoionization of 3,6-dihydro-*2H*-pyran.

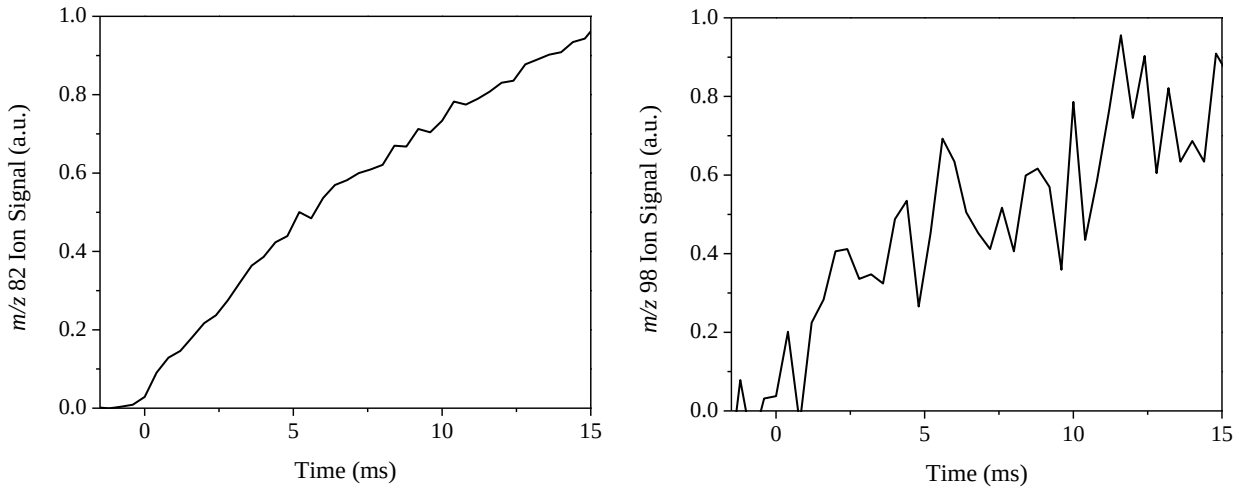

Figure 40. Time profiles of *m/z* = 82 (conjugate alkene) and *m/z* = 98 (cyclic ether / carbonyl) formed from oxidation of 3,6-dihydro-*2H*-pyranyl radicals.

The position of the sp^2 carbon relative to the ether group in 3,6-dihydro-*2H*-pyran simplifies the R + O_2 potential energy surfaces of the three radicals depicted in Figure 38, compared to the surfaces for radicals of 3,4-dihydro-*2H*-pyran. Neglecting reaction pathways involving vinylic hydrogen, oxirane-, oxetane-, and oxolane-type cyclic ether pathways exist across the three surfaces, in addition to a ketone-forming pathways. Accounting for both direct and sequential HO_2-forming mechanisms, and excluding vinylic H-abstraction, only four pathways exist across the three surfaces, all forming *2H*-pyran. The number of QOOH-mediated reactions leading to *m/z* = 98 cyclic ether or carbonyl species coincident with OH on the three surfaces is 9 (neglecting ring-opening reactions and vinylic H-abstraction). Representative reactions leading to *2H*-pyran (*m/z* = 82) and a bi-cyclic ether, 2,7-dioxabicyclo[4.1.0]hept-4-ene (*m/z* = 98), are depicted in Figure 41.

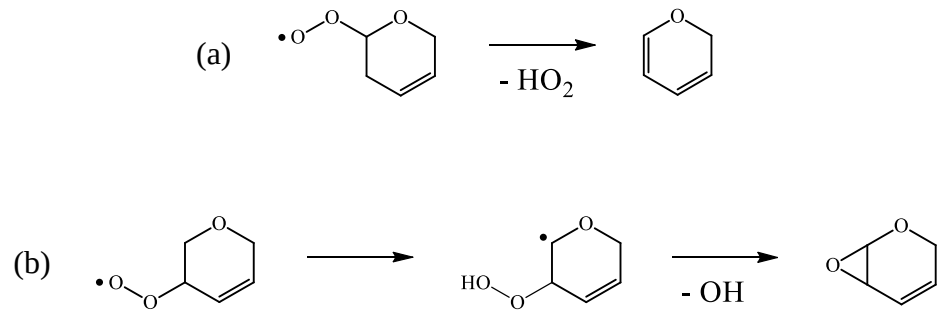

Figure 41. Representative reactions of peroxy radicals of 3,6-dihydro-*2H*-pyran leading to (a) *2H*-pyran (*m/z* = 82) and (b) 2,7-dioxabicyclo[4.1.0]hept-4-ene (*m/z* = 98).

3.3.3. Summary on RO_2 chemistry of intermediates from tetrahydropyran oxidation

Clear evidence of RO_2 chemistry is present in the Cl-initiated oxidation results of both 3,4-dihydro-*2H*-pyran and 3,6-dihydro-*2H*-pyran, evidenced in both the mass spectra and time profile measurements. Although no quantification of products is reported herein, which requires absolute photoionization cross-sections of the different isomers that comprise the mass channels, of particular significance is the comparable ion signal intensities for nominal *m/z* that are directly reflective of cyclic ether (or carbonyl) species being formed from R + O_2 indicating that QOOH formation is appreciable in such cases. Only marginal differences were noted in comparing the mass peaks appearing in the oxidation spectra of 3,4-dihydro-*2H*-pyran and 3,6-dihydro-*2H*-pyran. In both cases, the mass peak corresponding to conjugate alkene isomers (*m/z* = 82) remained the dominant signal. In contrast to the oxidation mass spectrum from cyclohexene, however, which is analogous with the exception of the ether group replacing a $–CH_2–$ group, the higher number of mass peaks indicates that ring-opening of the dihydro-*2H*-pyran isomers is likely to be significant at temperatures ≥ 700 K.

Several aspects of the results above are pertinent for the development of a comprehensive chemical kinetics model for tetrahydropyran that accounts for R + O_2 chemistry, which does not exist at present. First, in addition to radical-addition reactions involving the unsaturated 3,4-dihydro-*2H*-pyran (*m/z* = 84) and to 3,6-dihydro-*2H*-pyran (*m/z* = 84), R + O_2 reactions are also relevant given the detection of conjugate alkenes (*m/z* = 82). Similar reactions describing the formation and reaction of cyclic ether/carbonyl (*m/z* = 98) species are also relevant. The occurrence of these latter two types of species on identical timescales indicates that QOOH formation is relevant to 3,4-dihydro-*2H*-pyran and to 3,6-dihydro-*2H*-pyran oxidation. Second, given the tendency of ether functional groups to promote ring-opening reactions, secondary oxidation mechanisms involving the formation of linear radicals and subsequent R + O_2 chemistry. The complexity of the oxidation mass spectra lends credence to the existence of oxidation reactions involving ring-opened radicals.

4. CONCLUSIONS

Chlorine-atom-initiated oxidation experiments were conducted at 700 K and 10 Torr on primary oxidation intermediates of parent molecules 2,5-dimethylhexane, cyclohexane, and tetrahydropyran using multiplexed photoionization mass spectrometry. Product formation was probed in separate experiments on eight species: 2,5-dimethylhex-1-ene, 2,5-dimethylhex-2-ene, 2,5-dimethylhex-3-ene, 2,2,5,5-tetramethyltetrahydrofuran, cyclohexene, cyclohexene oxide, 3,4-dihydro-*2H*-pyran, and 3,6-dihydro-*2H*-pyran. Mass spectra and time profiles were measured and used to determine the presence of QOOH-mediated product formation from R + O_2 reactions, where R radicals were produced under pseudo-first-order conditions in reaction with Cl via RH + Cl → R + HCl. The results were analyzed for time-resolved ion signals of mass peaks corresponding to conjugate alkene formation, coincident with HO_2 in a chain-inhibiting step, and to cyclic ether/carbonyl formation, coincident with OH in a chain-propagating step.

In all cases, the eight primary oxidation intermediates were confirmed to undergo R + O_2 reactions similar to the degenerate chain-branching paradigm relied on to describe the chain-reactions occurring in alkanes. In addition, complex chemistry including ring-opening reactions of cyclic ether radicals – evidenced in the oxidation mass spectra of 2,2,5,5-tetramethyltetrahydrofuran, cyclohexene oxide, and 3,4- and 3,6-dihydro-*2H*-pyran – and rearrangement reactions are plausible. The implication of the results in confirming the presence of QOOH-mediated product formation from primary oxidation intermediates is an experimental basis emphasizing the need for the development of corresponding detailed sub-mechanisms, which are neglected in existing chemical kinetics models in favor of simplified sub-mechanisms. In general, the simplified sub-mechanisms of cyclic ethers and other primary oxidation intermediates largely center on initiation reactions with various radicals (OH, HO_2, CH_3, etc.) and in limited cases isomerization, homolysis, or radical-addition reactions are included. The utilization of lumped radicals, which undergo a small set of reactions that completely exclude reaction with O_2 and subsequent QOOH formation, is ubiquitous. Radicals of cyclic primary oxidation intermediates (i.e. cyclic ethers formed in chain-propagation steps) are commonly prescribed to only decompose via ring-opening into small-molecule radicals and stable species via β-scission.

The inherent complexity of comprehensive chemical kinetics models places some boundaries on development efforts, particularly for first-generation models where certain mechanistic information may be incomplete. However, expanding the boundaries to include detailed sub-mechanisms for primary oxidation intermediates is of potential benefit to increasing the fidelity and mechanistic rigor of such models. The definition of a primary oxidation intermediate herein refers to conjugate alkenes, cyclic ethers, or carbonyls formed directly from R + O_2 reactions. What defines the relevance of such species is the relative concentration compared to the parent molecule. In reactive environments where concentrations of primary oxidation intermediates approach parity with the depleting parent molecule, the details of the oxidation chemistry of the intermediate may not be a minor perturbation on the chemistry. In such cases understanding and accounting for initiation and other consumption reactions of primary oxidation intermediates will become important. Such reactions likely hold the most relevance for chemical kinetics model development efforts on lower reactivity molecules, including branched alkanes, alkenes, substituted aromatics, alcohols, and ketones where significant chain-inhibition and/or chain-propagation occurs (i.e. for species that do not exhibit pronounced NTC behavior).

5. REFERENCES

[1] C.K. Westbrook, *Proc. Combust. Inst.*, 28 (2000) 1563-1577.
[2] C.K. Westbrook, Y. Mizobuchi, T.J. Poinsot, P.J. Smith, E. Warnatz, *Proc. Combust. Inst.*, 30 (2005) 125-157.
[3] H.J. Curran, P. Gaffuri, W.J. Pitz, C.K. Westbrook, *Combust. Flame*, 114 (1998) 149-177.
[4] C.K. Westbrook, W.J. Pitz, O. Herbinet, H.J. Curran, E.J. Silke, *Combust. Flame*, 156 (2009) 181-199.
[5] B. Rotavera, P. Dagaut, E.L. Petersen, *Combust. Flame*, 161 (2014) 1146-1163.
[6] B. Rotavera, P. Diévart, C. Togbé, P. Dagaut, E.L. Petersen, *Proc. Combust. Inst.*, 33 (2011) 175-183.
[7] R.W. Walker, C. Morley, Chapter 1 - Basic Chemistry of Combustion, in: M.J. Pilling (Ed.) Comprehensive Chemical Kinetics, Elsevier, 1997, pp. 1-124.
[8] J. Zádor, R.X. Fernandes, C.A. Taatjes, *Prog. Energy Comb. Sci.*, 37 (2011) 371-421.
[9] M. Mehl, G. Vanhove, W.J. Pitz, E. Ranzi, *Combust. Flame*, 155 (2008) 756-772.
[10] R. Bounaceur, V. Warth, B. Sirjean, P.A. Glaude, R. Fournet, F. Battin-Leclerc, *Proc. Combust. Inst.*, 32 (2009) 387-394.
[11] F. Battin-Leclerc, A. Rodriguez, B. Husson, O. Herbinet, P.-A. Glaude, Z. Wang, Z. Cheng, F. Qi, *The Journal of Physical Chemistry A*, 118 (2014) 673-683.
[12] Z. Wang, L. Zhang, K. Moshammer, D.M. Popolan-Vaida, V.S.B. Shankar, A. Lucassen, C. Hemken, C.A. Taatjes, S.R. Leone, K. Kohse-Höinghaus, N. Hansen, P. Dagaut, S.M. Sarathy, *Combust. Flame*, 164 (2016) 386-396.
[13] E.J. Silke, W.J. Pitz, C.K. Westbrook, M. Ribaucour, *The Journal of Physical Chemistry A*, 111 (2007) 3761-3775.
[14] S.M. Sarathy, T. Javed, F. Karsenty, A. Heufer, W. Wang, S. Park, A. Elwardany, A. Farooq, C.K. Westbrook, W.J. Pitz, M.A. Oehlschlaeger, G. Dayma, H.J. Curran, P. Dagaut, *Combust. Flame*, 161 (2014) 1444-1459.
[15] Z. Serinyel, O. Herbinet, O. Frottier, P. Dirrenberger, V. Warth, P.A. Glaude, F. Battin-Leclerc, *Combust. Flame*, 160 (2013) 2319-2332.
[16] B. Rotavera, J. Zádor, O. Welz, L. Sheps, A.M. Scheer, J.D. Savee, M. Akbar Ali, T.S. Lee, B.A. Simmons, D.L. Osborn, A. Violi, C.A. Taatjes, *The Journal of Physical Chemistry A*, 118 (2014) 10188-10200.
[17] B. Rotavera, J.D. Savee, I.O. Antonov, R.L. Caravan, L. Sheps, D.L. Osborn, J. Zádor, C.A. Taatjes, *Proc. Combust. Inst.*, 36 (2017) 597-606.
[18] D.L. Osborn, P. Zou, H. Johnsen, C.C. Hayden, C.A. Taatjes, V.D. Knyazev, S.W. North, D.S. Peterka, M. Ahmed, S.R. Leone, *Rev. Sci. Inst.*, 79 (2008) 104103-104110.
[19] R. Atkinson, *Int. J. Chem. Kin.*, 19 (1987) 799-828.
[20] A.V. Baklanov, L.N. Krasnoperov, *The Journal of Physical Chemistry A*, 105 (2001) 97-103.
[21] B. Ghosh, D.K. Papanastasiou, J.B. Burkholder, *The Journal of Chemical Physics*, 137 (2012) 164315.
[22] P.A. Heimann, M. Koike, C.W. Hsu, D. Blank, X.M. Yang, A.G. Suits, Y.T. Lee, M. Evans, C.Y. Ng, C. Flaim, H.A. Padmore, *Review of Scientific Instruments*, 68 (1997) 1945-1951.
[23] S.R. Leone, M. Ahmed, K.R. Wilson, *Phys Chem Chem Phys*, 12 (2010) 6564-6578.
[24] I.O. Antonov, J. Kwok, J. Zádor, L. Sheps, *The Journal of Physical Chemistry A*, 119 (2015) 7742-7752.
[25] H. Sun, C.K. Law, *The Journal of Physical Chemistry A*, 114 (2010) 12088-12098.

[26] C.K. Westbrook, W.J. Pitz, S.M. Sarathy, M. Mehl, *Proc. Combust. Inst.*, 34 (2013) 3049-3056.
[27] A. El Bakli, M. Braun-Unkhoff, P. Dagaut, P. Frank, M. Cathonnet, *Proc. Combust. Inst.*, 28 (2000) 1631-1638.
[28] R.X. Fernandes, J. Zador, L.E. Jusinski, J.A. Miller, C.A. Taatjes, *Phys Chem Chem Phys*, 11 (2009) 1320-1327.
[29] A.M. Knepp, G. Meloni, L.E. Jusinski, C.A. Taatjes, C. Cavallotti, S.J. Klippenstein, *Phys Chem Chem Phys*, 9 (2007) 4315-4331.
[30] G. Dayma, P.A. Glaude, R. Fournet, F. Battin-Leclerc, *International Journal of Chemical Kinetics*, 35 (2003) 273-285.
[31] O. Lemaire, M. Ribaucour, M. Carlier, R. Minetti, *Combust. Flame*, 127 (2001) 1971-1980.
[32] M. Ribaucour, O. Lemaire, R. Minetti, *Proc. Combust. Inst.*, 29 (2002) 1303-1310.
[33] P. Dagaut, M. McGuinness, J.M. Simmie, M. Cathonnet, *Combustion Science and Technology*, 129 (1997) 1-16.
[34] L.-S. Tran, R. De Bruycker, H.-H. Carstensen, P.-A. Glaude, F. Monge, M.U. Alzueta, R.C. Martin, F. Battin-Leclerc, K.M. Van Geem, G.B. Marin, *Combust. Flame*, 162 (2015) 4283-4303.
[35] N.J. Labbe, V. Seshadri, T. Kasper, N. Hansen, P. Oßwald, P.R. Westmoreland, *Proc. Combust. Inst.*, 34 (2013) 259-267.

6. APPENDIX A: RATE PARAMETERS AND REACTIONS FOR OXIDATION INTERMEDIATES FROM R + O_2 REACTIONS

6.1. Sarathy et al., *Comb. Flame*, vol. 161, 2014, p. 1444 [14];

Table A1. Reactions involving 2,5-dimethylhex-1-ene (c8h16-1-25)

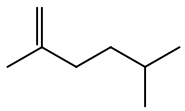

	Reaction	*A*	*n*	E_a (cal/mol)
1	h+**c8h16-1-25**=c8h17-25a	2.5E+11	0.51	2620
2	h+**c8h16-1-25**=c8h17-25b	4.2E+11	0.51	1230
3	**c8h16-1-25**+oh=*c8h15-1-25*+h2o	3.7E+08	1.61	-35
4	**c8h16-1-25**+ho2=*c8h15-1-25*+h2o2	5.1E+02	3.37	13720
5	**c8h16-1-25**+h=*c8h15-1-25*+h2	1.0E+07	2.40	4471
6	**c8h16-1-25**+ch3=*c8h15-1-25*+ch4	1.2E+01	3.46	5481
7	**c8h16-1-25**+o=*c8h15-1-25*+oh	4.4E+06	2.45	2830
8	**c8h16-1-25**+oh=ch2o+c7h15-2e	1.0E+11	0.00	-4000
9	**c8h16-1-25**+oh=ch3coch3+dc5h11	1.0E+11	0.00	-4000
10	**c8h16-1-25**+o=ch2o+c7h14-4-2	1.0E+11	0.00	-1050
11	**c8h16-1-25**+o=ch3coch2+dc5h11	1.0E+11	0.00	-1050
12	**c8h16-1-25**=ic4h7+ic4h9	1.0E+16	0.00	71000
13	**c8h16-1-25**=c3h6+cc5h10	4.0E+12	0.00	57629
14	c8h17oo-1-25<=>**c8h16-1-25**+ho2	8.5E+35	-7.22	41490
15	c8h17oo-2-25<=>**c8h16-1-25**+ho2	2.0E+43	-9.41	43490
16	**c8h16-1-25**+ho2=c8ooh1-25b	2.7E+03	2.50	10500
17	**c8h16-1-25**+ho2=c8ooh2-25a	2.7E+03	2.50	10500

Table A2. Reactions involving 2,5-dimethylhex-2-ene (c8h16-2-25)

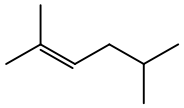

	Reaction	*A*	*n*	E_a (cal/mol)
1	h+**c8h16-2-25**=c8h17-25b	2.5E+11	0.51	2620
2	h+**c8h16-2-25**=c8h17-25c	2.5E+11	0.51	2620
3	**c8h16-2-25**+oh=*c8h15-1-25*+h2o	3.7E+08	1.61	-35
4	**c8h16-2-25**+ho2=*c8h15-1-25*+h2o2	5.1E+02	3.37	13720
5	**c8h16-2-25**+h=*c8h15-1-25*+h2	1.0E+07	2.40	4471
6	**c8h16-2-25**+ch3=*c8h15-1-25*+ch4	1.2E+01	3.46	5481
7	**c8h16-2-25**+o=*c8h15-1-25*+oh	4.4E+06	2.45	2830
8	**c8h16-2-25**+oh=ch3coch3+dc5h11	1.0E+11	0.00	-4000
9	**c8h16-2-25**+oh=ic3h7cho+ic4h9	1.0E+11	0.00	-4000
10	**c8h16-2-25**+o=ch3coch3+cc5h10	1.0E+11	0.00	-1050
11	**c8h16-2-25**+o=tc3h6cho+ic4h9	1.0E+11	0.00	-1050
12	**c8h16-2-25**=ic5h9+ic3h7	1.0E+16	0.00	71000
13	**c8h16-2-25**=ic4h8+ic4h8	4.0E+12	0.00	57629
14	c8h17oo-2-25<=>**c8h16-2-25**+ho2	1.0E+39	-8.11	42490
15	c8h17oo-3-25<=>**c8h16-2-25**+ho2	8.5E+35	-7.22	41490
16	**c8h16-2-25**+ho2=c8ooh2-25c	2.7E+03	2.50	10500
17	**c8h16-2-25**+ho2=c8ooh3-25b	2.7E+03	2.50	10500

Table A3. Reactions involving 2,5-dimethylhex-3-ene (c8h16-3-25)

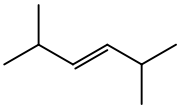

	Reaction	*A*	*n*	E_a (cal/mol)
1	h+**c8h16-3-25**=c8h17-25c	2.5E+11	0.51	2620
2	**c8h16-3-25**+oh=*c8h15-1-25*+h2o	3.7E+08	1.61	-35
3	**c8h16-3-25**+ho2=*c8h15-1-25*+h2o2	5.1E+02	3.37	13720
4	**c8h16-3-25**+h=*c8h15-1-25*+h2	1.0E+07	2.40	4471
5	**c8h16-3-25**+ch3=*c8h15-1-25*+ch4	1.2E+01	3.46	5481
6	**c8h16-3-25**+o=*c8h15-1-25*+oh	4.4E+06	2.45	2830
7	**c8h16-3-25**+oh=ic3h7cho+ic4h9	1.0E+11	0.00	-4000
8	**c8h16-3-25**+o=ic3h7cho+ic4h8	1.0E+11	0.00	-1050
9	**c8h16-3-25**=c7h13-1-2+ch3	1.0E+16	0.00	71000
10	**c8h16-3-25**=ic4h8+ic4h8	4.0E+12	0.00	57629
11	c8h17oo-3-25<=>**c8h16-3-25**+ho2	1.0E+39	-8.11	42490
12	**c8h16-3-25**+ho2=c8ooh3-25d	2.7E+03	2.50	10500

Table A4. Reactions involving lumped alkenyl radicals 2,5-dimethylhex-A-en-B-yl (c8h15-1-25); A ≡ location of C=C bond, B ≡ location of unpaired electron on carbon atom;

	Reaction	*A*	*n*	E_a (cal/mol)
1	c8h16-1-25+oh=**c8h15-1-25**+h2o	3.7E+08	1.61	-35
2	c8h16-2-25+oh=**c8h15-1-25**+h2o	3.7E+08	1.61	-35
3	c8h16-3-25+oh=**c8h15-1-25**+h2o	3.7E+08	1.61	-35
4	c8h16-1-25+ho2=**c8h15-1-25**+h2o2	5.1E+02	3.37	13720
5	c8h16-2-25+ho2=**c8h15-1-25**+h2o2	5.1E+02	3.37	13720
6	c8h16-3-25+ho2=**c8h15-1-25**+h2o2	5.1E+02	3.37	13720
7	c8h16-1-25+h=**c8h15-1-25**+h2	1.0E+07	2.40	4471
8	c8h16-2-25+h=**c8h15-1-25**+h2	1.0E+07	2.40	4471
9	c8h16-3-25+h=**c8h15-1-25**+h2	1.0E+07	2.40	4471
10	c8h16-1-25+ch3=**c8h15-1-25**+ch4	1.2E+01	3.46	5481
11	c8h16-2-25+ch3=**c8h15-1-25**+ch4	1.2E+01	3.46	5481
12	c8h16-3-25+ch3=**c8h15-1-25**+ch4	1.2E+01	3.46	5481
13	c8h16-1-25+o=**c8h15-1-25**+oh	4.4E+06	2.45	2830
14	c8h16-2-25+o=**c8h15-1-25**+oh	4.4E+06	2.45	2830
15	c8h16-3-25+o=**c8h15-1-25**+oh	4.4E+06	2.45	2830
16	**c8h15-1-25+ho2**=ac3h5cho+ic4h9+oh	9.6E+12	0.00	0
17	**c8h15-1-25+ch3o2**=ac3h5cho+ic4h9+ch3o	9.6E+12	0.00	0
18	**c8h15-1-25+c2h5o2**=ac3h5cho+ic4h9+c2h5o	9.6E+12	0.00	0
19	**c8h15-1-25**=ic3h7+c5h81-3	2.5E+13	0.00	30000
20	**c8h15-1-25**=c3h4-p+dc5h11	2.5E+13	0.00	30000
21	**c8h15-1-25**=c3h5-t+ac5h10	2.5E+13	0.00	30000
22	**c8h15-1-25**=ic4h7+ic4h8	2.5E+13	0.00	30000
23	**c8h15-1-25**=ic5h9+c3h6	2.5E+13	0.00	30000

Table A5. Reactions involving 2,2,5,5-tetramethyltetrahydrofuran (c8h16o2-5-25)

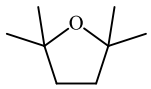

	Reaction	*A*	*n*	E_a (cal/mol)
1	c8ooh2-25e=**c8h16o2-5-25**+oh	2.7E+10	0.00	7000
2	**c8h16o2-5-25**+oh=ch3coch3+ic5h9+h2o	5.0E+12	0.00	0
3	**c8h16o2-5-25**+ho2=ch3coch3+ic5h9+h2o2	1.0E+13	0.00	17700

6.2. Serinyel et al., *Comb. Flame*, vol. 160, 2013 p. 2319 [15];

Table A6. Reactions involving cyclohexene (C6H10Z#6)

	Reaction	*A*	*n*	E_a (cal/mol)
1	RC1C6H11#6=>R1H+**C6H10Z#6**	8.90E+11	0.83	36340
2	RC2C6H11O2#6U=>**C6H10Z#6**+R3OOH	8.50E+12	0.00	32100
3	RC1C6H11#6+O2=**C6H10Z#6**+R3OOH	3.88E+12	0.00	5000
4	RC1C6H11#6+O2=>**C6H10Z#6**+R3OOH	7.90E+12	0.00	5000
5	**C6H10Z#6**=C2H4Z+C4H6Z2	5.50E+12	0.76	62450
6	**C6H10Z#6**=C6H8#6-13+H2	5.0E+13	0.00	61700
7	**C6H10Z#6**=*RC1C6H9#6Z*+R1H	1.2E+15	0.00	98900
8	**C6H10Z#6**=*RC2C6H9#6Y*+R1H	1.2E+15	0.00	83200
9	**C6H10Z#6**=*RC3C6H9#6V*+R1H	1.1E+15	0.00	107800
10	**C6H10Z#6**+O2=*RC1C6H9#6Z*+R3OOH	4.0E+13	0.00	50700
11	**C6H10Z#6**+O2=*RC2C6H9#6Y*+R3OOH	7.2E+13	0.00	34800
12	**C6H10Z#6**+O2=*RC3C6H9#6V*+R3OOH	2.0E+13	0.00	59100
13	**C6H10Z#6**+**C6H10Z#6**=*RC1C6H9#6Z*+RC1C6H11#6	1.9E+13	0.00	66600
14	**C6H10Z#6**+**C6H10Z#6**=*RC1C6H9#6Z*+RC1C6H11#6	1.9E+13	0.00	66600
15	**C6H10Z#6**+**C6H10Z#6**=*RC2C6H9#6Y*+RC1C6H11#6	1.9E+13	0.00	50900
16	**C6H10Z#6**+**C6H10Z#6**=*RC2C6H9#6Y*+RC1C6H11#6	1.9E+13	0.00	50900
17	**C6H10Z#6**+**C6H10Z#6**=*RC3C6H9#6V*+RC1C6H11#6	3.9E+13	0.00	75500
18	**C6H10Z#6**+**C6H10Z#6**=*RC3C6H9#6V*+RC1C6H11#6	3.9E+13	0.00	75500
19	**C6H10Z#6**+C4H6Z2=*RC2C6H9#6Y*+R122C4H7Y	4.5E+13	0.00	32600
20	**C6H10Z#6**+C2H4Z=*RC2C6H9#6Y*+R11C2H5	6.2E+13	0.00	47300
21	**C6H10Z#6**+B1O=>C2H3CHOZ+R1H+R104C3H5Y	1.20E+05	2.56	-1130
22	**C6H10Z#6**+R2OH=RC6C6H10OH#6	2.8E+12	0.00	-1040
23	**C6H10Z#6**+R3OOH=RC7C6H10OOH#6	1.0E+12	0.00	12000
24	**C6H10Z#6**+B1O=>*RC1C6H9#6Z*+R2OH	5.2E+13	0.00	5200
25	**C6H10Z#6**+B1O=>*RC2C6H9#6Y*+R2OH	1.8E+11	0.70	3250
26	**C6H10Z#6**+B1O=>*RC3C6H9#6V*+R2OH	1.2E+11	0.70	7630
27	**C6H10Z#6**+R1H=>*RC1C6H9#6Z*+H2	1.8E+07	2.00	5000
28	**C6H10Z#6**+R1H=>*RC2C6H9#6Y*+H2	1.1E+05	2.50	-1900
29	**C6H10Z#6**+R1H=>*RC3C6H9#6V*+H2	8.2E+05	2.50	9790
30	**C6H10Z#6**+R2OH=>*RC1C6H9#6Z*+H2O	5.2E+06	2.00	-770
31	**C6H10Z#6**+R2OH=>*RC2C6H9#6Y*+H2O	6.0E+06	2.00	-1520
32	**C6H10Z#6**+R2OH=>*RC3C6H9#6V*+H2O	2.2E+06	2.00	1450
33	**C6H10Z#6**+R3OOH=>*RC1C6H9#6Z*+H2O2	8.0E+11	0.00	15500
34	**C6H10Z#6**+R3OOH=>*RC2C6H9#6Y*+H2O2	1.3E+04	2.60	12400
35	**C6H10Z#6**+R3OOH=>*RC2C6H9#6Y*+H2O2	8.0E+11	0.00	13500
36	**C6H10Z#6**+R3OOH=>*RC3C6H9#6V*+H2O2	0.0E+00	0.00	0
37	**C6H10Z#6**+R4CH3=>*RC1C6H9#6Z*+CH4	4.0E+11	0.00	9600
38	**C6H10Z#6**+R4CH3=>*RC2C6H9#6Y*+CH4	2.0E+11	0.00	7300
39	**C6H10Z#6**+R4CH3=>*RC3C6H9#6V*+CH4	2.0E+00	3.50	11700

Table A7. Reactions involving radical RC1C6H9#6Z ≡ cyclohex-1-en-4-yl 

	Reaction	*A*	*n*	E_a (cal/mol)
1	C6H10Z#6=**RC1C6H9#6Z**+R1H	1.2E+15	0.00	98900
2	C6H10Z#6+O2=**RC1C6H9#6Z**+R3OOH	4.0E+13	0.00	50700
3	C6H10Z#6+C6H10Z#6=**RC1C6H9#6Z**+RC1C6H11#6	1.9E+13	0.00	66600
4	C6H10Z#6+B1O=>**RC1C6H9#6Z**+R2OH	5.2E+13	0.00	5200
5	C6H10Z#6+R1H=>**RC1C6H9#6Z**+H2	1.8E+07	2.00	5000
6	C6H10Z#6+R2OH=>**RC1C6H9#6Z**+H2O	5.2E+06	2.00	-770
7	C6H10Z#6+R3OOH=>**RC1C6H9#6Z**+H2O2	8.0E+11	0.00	15500
8	C6H10Z#6+R4CH3=>**RC1C6H9#6Z**+CH4	4.0E+11	0.00	9600
9	**RC1C6H9#6Z**+R3OOH=>R2OH+R5CHO+C5H8#5	1E+14	0.00	0
10	**RC1C6H9#6Z**+O2=R3OOH+C6H8#6-14	9.6E+12	0.00	5000
11	**RC1C6H9#6Z**+O2=R3OOH+C6H8#6-13	9.6E+12	0.00	2500
12	**RC1C6H9#6Z**+R3OOH=>R2OH+R13CH2CHO+C4H6Z2	1E+15	-0.80	0
13	**RC1C6H9#6Z**=RC2C6H9#6Y	1.9E+13	0.00	36700
14	**RC1C6H9#6Z**=RC6H9ZX	2.75E+12	0.62	30810
15	C4H6Z2+R10C2H3V=>**RC1C6H9#6Z**	7.7E+13	-1.35	3994

Table A8. Reactions involving radical cyclohex-1-en-3-yl (RC2C6H9#6Y) 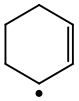

	Reaction	*A*	*n*	E_a (cal/mol)
1	C6H10Z#6=**RC2C6H9#6Y**+R1H	1.2E+15	0.00	83200
2	C6H10Z#6+O2=**RC2C6H9#6Y**+R3OOH	7.2E+13	0.00	34800
3	C6H10Z#6+C6H10Z#6=**RC2C6H9#6Y**+RC1C6H11#6	1.9E+13	0.00	50900
4	C6H10Z#6+C4H6Z2=**RC2C6H9#6Y**+R122C4H7Y	4.5E+13	0.00	32600
5	C6H10Z#6+C2H4Z=**RC2C6H9#6Y**+R11C2H5	6.2E+13	0.00	47300
6	C6H10Z#6+B1O=>**RC2C6H9#6Y**+R2OH	1.8E+11	0.70	3250
7	C6H10Z#6+R1H=>**RC2C6H9#6Y**+H2	1.1E+05	2.50	-1900
8	C6H10Z#6+R2OH=>**RC2C6H9#6Y**+H2O	6.0E+06	2.00	-1520
9	C6H10Z#6+R3OOH=>**RC2C6H9#6Y**+H2O2	1.3E+04	2.60	12400
10	C6H10Z#6+R3OOH=>**RC2C6H9#6Y**+H2O2	8.0E+11	0.00	13500
11	C6H10Z#6+R4CH3=>**RC2C6H9#6Y**+CH4	2.0E+11	0.00	7300
12	**RC2C6H9#6Y**+R3OOH=>R2OH+R5CHO+C5H8#5	1E+14	0.00	0
13	**RC2C6H9#6Y**+O2=R3OOH+C6H8#6-13	9.6E+12	0.00	15160
14	**RC2C6H9#6Y**+R3OOH=>R2OH+C2H4Z+B2CO+R104C3H5Y	1E+15	-0.80	0
15	RC1C6H9#6Z=**RC2C6H9#6Y**	1.9E+13	0.00	36700
16	RC3C6H9#6V=**RC2C6H9#6Y**	1.3E+13	0.00	44500
17	**RC2C6H9#6Y**=>RC6H9ZY	2.75E+12	0.62	30810

Table A9. Reactions involving radical cyclohex-1-en-1-yl (RC3C6H9#6V)

	Reaction	*A*	*n*	E_a (cal/mol)
1	C6H10Z#6=**RC3C6H9#6V**+R1H	1.1E+15	0.00	107800
2	C6H10Z#6+O2=**RC3C6H9#6V**+R3OOH	2.0E+13	0.00	59100
3	C6H10Z#6+C6H10Z#6=**RC3C6H9#6V**+RC1C6H11#6	3.9E+13	0.00	75500
4	C6H10Z#6+B1O=>**RC3C6H9#6V**+R2OH	1.2E+11	0.70	7630
5	C6H10Z#6+R1H=>**RC3C6H9#6V**+H2	8.2E+05	2.50	9790
6	C6H10Z#6+R2OH=>**RC3C6H9#6V**+H2O	2.2E+06	2.00	1450
7	C6H10Z#6+R3OOH=>**RC3C6H9#6V**+H2O2	0.0E+00	0.00	0
8	C6H10Z#6+R4CH3=>**RC3C6H9#6V**+CH4	2.0E+00	3.50	11700
9	**RC3C6H9#6V**+R3OOH=>R2OH+R10C2H3V+C2H4Z+CH2COZ	1E+15	-0.80	0
10	**RC3C6H9#6V**=RC2C6H9#6Y	1.3E+13	0.00	44500

Table A10. Reactions involving cyclohexene oxide / 1,2-epoxycyclohexane (C6H10#6O#3)

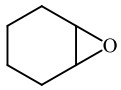

	Reaction	*A*	*n*	E_a (cal/mol)
1	**C6H10#6O#3**+R1H=>H2+*RC6H9#6OK*	8.40E+06	2	2400
2	**C6H10#6O#3**+R2OH=>H2O+*RC6H9#6OK*	2.20E+06	2	-1870
3	**C6H10#6O#3**+R3OOH=>H2O2+*RC6H9#6OK*	2.00E+12	0	14000
4	**C6H10#6O#3**+R4CH3=>CH4+*RC6H9#6OK*	2.00E+11	0	7900
5	**C6H10#6O#3**+R8CH3OO=>CH3OOH+*RC6H9#6OK*	3.00E+12	0	15000
6	**C6H10#6O#3**+R11C2H5=>C2H6+*RC6H9#6OK*	2.00E+11	0	9200

Table A11. Reactions involving lumped cyclic ether radicals (RC6H9#6OK).

	Reaction	*A*	*n*	E_a (cal/mol)
1	**RC6H9#6OK**<=>RC6H9OZ	2.75E+12	0.624	30800
2	**RC6H9#6OK**+O2<=>C6H8O#6KZ+R3OOH	3.88E+12	0	5000

6.3. Silke et al., *J. Phys. Chem. A*, vol. 111, 2007 p. 3761 [13];

Table A12. Reactions involving cyclohexene (cychexene)

	Reaction	*A*	*n*	E_a (cal/mol)
1	ic5h7 + **cychexene** = ic5h8 + *cyhx1n4j*	3.69E+00	3.31	13000
2	c2h3chcho + **cychexene** = ac3h5cho + *cyhx1n4j*	1.05E+00	3.31	15000
3	c2h3chcho + **cychexene** = ac3h5cho + *cyhx1n3j*	1.05E+00	3.31	15000
4	chxj2ch2q = **cychexene** + ch2o + oh	2.60E+14	0.036	33448.5
5	chxyco-2 = **cychexene** + ch2o	1.00E+17	0	88000
6	chxo2j = **cychexene** + ho2	3.85E+12	0	29000
7	**cychexene** + ho2 = chx1q2j	8.00E+10	0	6000
8	**cychexene** + h = chxrad	6.25E+11	0.51	2620
9	**cychexene** = c4h6 + c2h4	4.00E+12	0	57400
10	**cychexene** + h = *cyhx1n3j* + h2	1.00E+05	2.5	-1912
11	**cychexene** + h = *cyhx1n4j* + h2	2.30E+06	2.49	4124
12	**cychexene** + ch3 = *cyhx1n3j* + ch4	2.00E-01	3.5	4046.1
13	**cychexene** + ch3 = *cyhx1n4j* + ch4	1.08E+05	2.26	7287
14	**cychexene** + o = *cyhx1n3j* + oh	1.59E+11	0.7	3107.07
15	**cychexene** + o = *cyhx1n4j* + oh	1.91E+05	2.71	2106
16	**cychexene** + oh = *cyhx1n3j* + h2o	6.34E+06	2	-1434
17	**cychexene** + oh = *cyhx1n4j* + h2o	3.60E+06	2	-1133
18	**cychexene** + ho2 = *cyhx1n3j* + h2o2	1.36E+04	2.5	10113.8
19	**cychexene** + ho2 = *cyhx1n4j* + h2o2	2.24E+13	0	17686

Table A13. Reactions involving radical cyclohex-1-en-4-yl (cyhx1n4j)

	Reaction	*A*	*n*	E_a (cal/mol)
1	ic5h7 + cychexene = ic5h8 + **cyhx1n4j**	3.69E+00	3.31	13000
2	c2h3chcho + cychexene = ac3h5cho + **cyhx1n4j**	1.05E+00	3.31	15000
3	cyhx13ene + h = **cyhx1n4j**	1.25E+12	0.51	2620
4	hx14en6j = **cyhx1n4j**	1.00E+08	0.86	5900

Table A14. Reactions involving radical cyclohex-1-en-3-yl (cyhx1n3j)

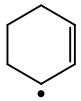

	Reaction	*A*	*n*	E_a (cal/mol)
1	ic5h7 + cychexene = ic5h8 + **cyhx1n3j**	3.69E+00	3.31	13000
2	c2h3chcho + cychexene = ac3h5cho + **cyhx1n3j**	1.05E+00	3.31	15000
3	**cyhx1n3j** + o2 = cyhx13ene + ho2	2.10E+09	0	0
4	**cyhx1n3j** + ho2 = cyhx1n3oj + oh	7.00E+12	0	-1000
5	cyhx13ene + h = **cyhx1n3j**	1.25E+12	0.51	1500
6	hx13en6j = **cyhx1n3j**	1.00E+08	0.86	5900

Table A15. Reactions involving cyclohexene oxide / 1,2-epoxycyclohexane (chxyo12)

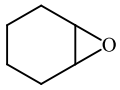

	Reaction	*A*	*n*	E_a (cal/mol)
1	chx1q2j = **chxyo12** + oh	5.80E+12	0	13400
2	**chxyo12**+oh=*chx1*o2j*+h2o	3.40E+06	1.9	-1451
3	**chxyo12**+h=*chx1*o2j*+h2o	1.20E+06	2.4	2583
4	**chxyo12**+ch3=*chx1*o2j*+ch4	1.79E+04	2.33	6147
5	**chxyo12**+ho2=*chx1*o2j*+h2o2	3.00E+04	2.5	12260
6	hco+**chxyo12**=chxcho2oj	1.00E+11	0	5500

Table A16. Reactions involving lumped cyclohexene oxide radicals (chx1*o2j);

	Reaction	*A*	*n*	E_a (cal/mol)
1	**chx1*o2j** = c2h3+ch2co+c2h4	8.11E+13	0.508	28517
2	**chx1*o2j** = c2h4+c2h4+hcco	4.24E+15	0.195	36287
3	hx1n3*o6j = **chx1*o2j**	1.00E+08	0.86	5900

DISTRIBUTION

4	University of Georgia Attn: Brandon Rotavera 110 Riverbend Road Athens, GA 30602		
1	MS0899	Technical Library	9536 (electronic copy)
1	MS9055	Craig A. Taatjes	8353


Sandia National Laboratories